Seismic imaging of a convergent continental margin and plateau in the central Andes (Andean Continental Research Project 1996 (ANCORP'96))

ANCORP Working Group

ANCORP (Andean Continental Research Project) Working Group: Onno Oncken, Stephan Sobolev, Manfred Stiller, Günter Asch, Christian Haberland, James Mechie, Xiaohui Yuan (GeoForschungsZentrum Potsdam, Potsdam, Germany); Ewald Lüschen (Universität München, Munich, Germany); Peter Giese, Peter Wigger, Stefan Lueth, Ekkehard Scheuber, Hans-Jürgen Götze, Heinrich Brasse, Stefan Buske, Mi-Kyung Yoon, Serge Shapiro (Freie Universität Berlin, Berlin, Germany); Andreas Rietbrock (University of Potsdam, Institute of Geosciences, Potsdam, Germany); Guillermo Chong, Hans-Gerhard Wilke, Gabriel Gonzalez (Universidad Católica del Norte, Antofagasta, Chile); Patricio Bravo, Hugo Vieytes (Empresa Nacional Del Petróleo, Punta Arenas, Chile); Eloy Martinez (Chaco-SA, Santa Cruz, Bolivia); Reinhard Rössling (SERGEOMIN, La Paz, Bolivia); and Edgar Ricaldi (Universidad Mayor de San Andres, La Paz, Bolivia).

Received 18 January 2002; revised 22 July 2002; accepted 27 January 2003; published 3 July 2003.

[1] A 400-km-long seismic reflection profile (Andean Continental Research Project 1996 (ANCORP'96)) and integrated geophysical experiments (wide-angle seismology, passive seismology, gravity, and magnetotelluric depth sounding) across the central Andes (21°S) observed subduction of the Nazca plate under the South American continent. An east dipping reflector (Nazca Reflector) is linked to the down going oceanic crust and shows increasing downdip intensity before gradual breakdown below 80 km. We interpret parts of the Nazca Reflector as a fluid trap located at the front of recent hydration and shearing of the mantle, the fluids being supplied by dehydration of the oceanic plate. Patches of bright (Quebrada Blanca Bright Spot) to more diffuse reflectivity underlie the plateau domain at 15–30 km depth. This reflectivity is associated with a low-velocity zone, *P* to *S* wave conversions, the upper limits of high conductivity and high V_p/V_s ratios, and to the occurrence of Neogene volcanic rocks at surface. We interpret this feature as evidence of widespread partial melting of the plateau crust causing decoupling of the upper and lower crust during Neogene shortening and plateau growth. The imaging properties of the continental Moho beneath the Andes indicate a broad transitional character of the crust-mantle boundary owing to active processes like hydration of mantle rocks (in the cooler parts of the plate margin system), magmatic underplating and intraplating under and into the lowermost crust, mechanical instability at Moho, etc. Hence all first-order features appear to be related to fluid-assisted processes in a subduction setting. *INDEX TERMS:* 5475 Planetology: Solid Surface Planets: Tectonics (8149); 8110 Tectonophysics: Continental tectonics—general (0905); 9360 Information Related to Geographic Region: South America; 8150 Tectonophysics: Evolution of the Earth: Plate boundary—general (3040); 5480 Planetology: Solid Surface Planets: Volcanism (8450); *KEYWORDS:* Andes, reflection seismics, plateau formation, crustal melting, convergent plate margin, subduction

Citation: ANCORP Working Group, Seismic imaging of a convergent continental margin and plateau in the central Andes (Andean Continental Research Project 1996 (ANCORP'96)), *J. Geophys. Res.*, *108*(B7), 2328, doi:10.1029/2002JB001771, 2003.

1. Introduction

[2] Next to continental collisional belts, convergent ocean-continent margins are a key site of growth of continental crust and of orogeny involving a variety of processes, most of which operate at exceptionally high rates. While this is a well established corollary of plate tectonic theory [e.g., *Isacks et al.*, 1968; *Dewey and Bird*, 1970] surprisingly little highly resolved deep evidence has been presented that corroborates the suggested processes from images of the deep interior of an active subduction setting and of the related processes in the overlying plate. Most of the present knowledge on processes inferred to operate at depth is from indirect surface-based observations (seismicity, geochemical data from active volcanism, GPS, etc.) or from fossil deeply eroded convergent margins and orogenic belts that, however, were mostly heavily overprinted during exhumation. The experiments across the North American margin, which are the only integrated geophysical surveys across the offshore and onshore parts of a convergent continental margin [e.g., *Green et al.*, 1986; *Clowes et al.*, 1987], were the first to show a dipping slab to some 30–40 km beneath the forearc and a more highly resolved image of accretionary structure and processes in the overlying continent.

0148-0227/03/2002JB001771$09.00

[3] In contrast to the North American margin, which is largely controlled by collision with complex terranes, the South American Andes are a more simple convergent system lacking continental accretion and continent-continent collision in the Mesozoic and Cenozoic. Our key motivation to study the central Andes, moreover, is its character as the type subduction related cordilleran mountain belt [i.e., *Dewey and Bird*, 1970] that shows the entire set of features associated with long lasting active subduction at a convergent continental margin. Some 200 Ma continuous subduction of various oceanic plates beneath the South American continent has resulted in the largest cordilleran type orogenic belt with the Earth's largest plateau formed without continent-continent collision [*Isacks*, 1988; *Allmendinger et al.*, 1997; *Allmendinger and Gubbels*, 1996; *Kley and Monaldi*, 1998; *Lamb and Hoke*, 1997; *Lamb*, 2000]. Moreover, it has been pointed out that the central Andes are a type setting showing continuous subduction erosion of the upper plate crust during the entire subduction cycle [*James*, 1971; *Rutland*, 1981; *Von Huene and Scholl*, 1991].

[4] In 1996 the international Andean Continental Research Project (ANCORP) experiment (a German-Chilean-Bolivian cooperation involving academic, governmental, and commercial institutions) was carried out. Its aim was to image the subduction zone, the traces of active magmatism, the geometry of crustal thickening and plateau formation, and the process of subduction-erosion at this particular convergent margin. The experiment consisted of an ''active'' component comprising the acquisition of very deep seismic images along a 400-km-long integrated seismic reflection and refraction profile across the central Andes in northern Chile and southern Bolivia (Figure 1) and a ''passive'' component consisting of the recording of earthquakes during a 3-month campaign.

[5] First results from the ANCORP experiment across the central Andes indicated that the potential to image the deep continuation of the Wadati-Benioff zone and the related upper plate processes might be better than previously assumed [*ANCORP Working Group*, 1999]. In this paper, we present the completely processed seismic reflection and refraction data from the integrated ANCORP experiments. Our data are complemented by recently published receiver function analyses [*Yuan et al.*, 2000, 2002], gravity and magnetotelluric data along the same transect [*Goetze and Kirchner*, 1997; *Brasse et al.*, 2002]. Additionally, the section links to offshore reflection profiles of project Crustal Investigations Off- and On-Shore Nazca/Central Andes 1995 (CINCA'95) [*CINCA Working Group*, 1997] that continue to the oceanic Nazca plate. The section at 21°S is also covered by an abundance of earlier data that enable a comprehensive geophysical view [*Schmitz et al.*, 1999; *Patzwahl et al.*, 1999; *Schmitz and Kley*, 1997] and that probably make the central Andes the geophysically most densely covered convergent continental margin.

2. Central Andean Geological Framework

[6] The Andes are the Earth's largest active subduction-controlled orogen with a length of more than 7000 km. In their central parts (16–28°S), convergence resulted in formation of a large plateau that is highly symmetric in plan view about the Arica bend (Andean orocline). The plateau is flanked, at both ends, by recent flat slab subduction. At 21°S, the latitude of the southern Altiplano plateau, the oceanic Nazca plate dips at some 20–30° beneath the South American plate as evidenced from the trace of the seismological Wadati-Benioff zone [*Cahill and Isacks*, 1992; *Comte et al.*, 1994; *Comte and Suárez*, 1995; *ANCORP Working Group*, 1999]. The recent convergence rate between the Nazca plate and South America of 6.6 cm/yr from GPS data [*Angermann et al.*, 1999] resulted after continuous slowing from a peak of some 15 cm/yr during the early Miocene [*DeMets et al.*, 1990; *Somoza*, 1998]. Convergence with South America since that time moreover has proceeded with minor, only slightly variable, oblique convergence.

[7] The uplift of the central Andean cordillera started in early Tertiary times [*Lamb et al.*, 1997] with a focused plateau development since the Miocene during peak convergence rates [*Allmendinger and Gubbels*, 1996; *Allmendinger et al.*, 1997]. This period of enhanced plateau uplift shows a complex lateral and temporal relation to magmatism. In the Miocene, a major ignimbrite flare-up is suggested to have been the consequence of steepening slab geometry [*Isacks*, 1988; *Kay and Kay*, 1993; *Allmendinger et al.*, 1997; *Scheuber and Giese*, 1999] that initiated the main stage of plateau evolution. After an earlier stage of shortening (up to ~10 Ma) that was mainly restricted to the Eastern and Western Cordillera confining the plateau, the zone of active shortening migrated from the plateau into the sub-Andean [*Allmendinger and Gubbels*, 1996]. Here recent deformation at the orogenic tip proceeds with active crustal seismicity and shortening rates in the order of 0.5–2 cm/yr as shown from GPS data [*Klotz et al.*, 1999; *Hindle et al.*, 2002].

[8] As a result, the Andes show extreme dimensions in their central part with a mountain belt width of more than 800 km and the Altiplano/Puna plateaus situated at an average elevation of 3800–4500 m between the volcanic Western Cordillera and the Eastern Cordillera. The related crustal thickness, as observed from wide-angle and teleseismic data, reaches 65–75 km in the back-arc area beneath the Altiplano [*Wigger et al.*, 1994; *Beck et al.*, 1996; *Myers et al.*, 1998; *Schmitz et al.*, 1999; *Yuan et al.*, 2000, 2002; *Swenson et al.*, 2000]. Only some 70% of this value has so far been convincingly explained as the result of well documented crustal shortening [*Kley and Monaldi*, 1998; *Allmendinger et al.*, 1997; *Giese et al.*, 1999; *Kley et al.*, 1999]. Crustal shortening responsible for plateau evolution is confined to the back-arc area where the thin skinned fold and thrust belt of the Eastern Cordillera and sub-Andean zone at ~20°S accumulated some 150–200 km shortening [*Kley and Monaldi*, 1998; *Baby et al.*, 1997] versus some 85 km in the plateau itself [*Lamb and Hoke*, 1997; *Lamb*, 2000]. In contrast to the more symmetrically deformed Puna plateau, the Altiplano therefore was suggested to be the result of simple shear crustal thickening due to underthrusting of the Altiplano area by the Brazilian shield from the east [e.g., *Allmendinger and Gubbels*, 1996; *Allmendinger et al.*, 1997]. Rather than forming a fold and thrust belt as in the sub-Andean, deformation of the internal parts of the plateau mainly involved localized deformation at major fault systems (e.g., Uyuni-Kenayani fault zone in the southern Altiplano) with formation of intervening inter-

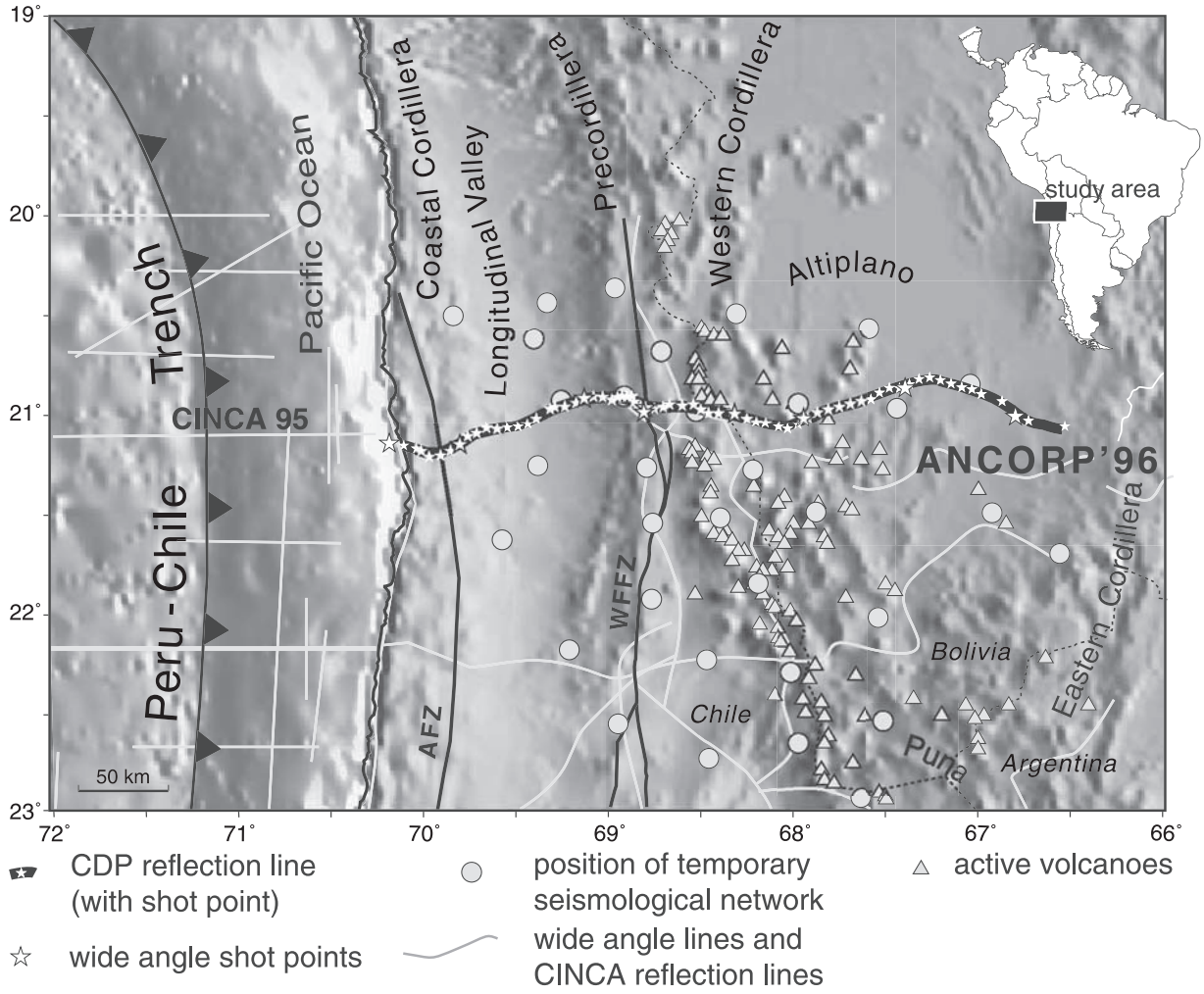

Figure 1. Location map of the ANCORP 96 reflection and refraction profile, the marine CINCA'95 lines [*CINCA Working Group*, 1997], the temporary passive seismological network, and earlier onshore wide-angle lines referred to in the text [from *Wigger et al.*, 1994]. Inset shows location of transect with respect to South America.

nally drained basins containing thick Cenozoic deposits [*Lamb*, 2000].

[9] On its western margin, the plateau includes the recent magmatic arc, which is active since Middle Miocene times [*Baker and Francis*, 1978]. Deformation of the adjoining forearc is only minor and shows a complex pattern involving deformation partitioning at several scales and reactivation of earlier major subvertical strike slip fault systems (Precordilleran fault system [*Reutter et al.*, 1996]; Atacama fault system [*Scheuber et al.*, 1994; *Delouis et al.*, 1998]). The forearc topography is strongly segmented with (1) the steep western flank of the Altiplano; (2) the nearly flat Longitudinal Valley and low Coastal Cordillera, both with some Neogene cover; and (3) the spectacular escarpment of more than 1000 m at the coast linking to the steeply tapered extensional offshore forearc. No accretionary wedge is developed. As evidenced by marine reflection profiles collected during the CINCA experiment in 1995 (between 19°S and 26°S), features suggesting tectonic erosion are particularly well developed in the offshore area [*Von Huene et al.*, 1999]. The eastward migration of the volcanic front from the Coastal Cordillera since the Jurassic to its present position in the Western Cordillera indicates that more than 200 km of continental material in an E-W section have been tectonically eroded and subducted [*Rutland*, 1971; *Ziegler et al.*, 1981; *Scheuber et al.* 1994].

3. Experimental Setup

[10] The survey was conducted from 15 September to 20 November 1996, by cooperating institutions from Germany, Chile, and Bolivia. The onshore reflection and wide-angle line continued previously acquired offshore reflection data (CINCA'95 project) at 21°S and extends E-W from the coast for about 400 km across the Coastal Cordillera, the Longitudinal Valley, the Precordillera, the Western Cordillera, and the Altiplano (Figure 1). Earlier wide-angle data [*Wigger et al.*, 1994; *Schmitz and Kley*, 1997; *Schmitz et al.*, 1999; *Patzwahl et al.*, 1999] have imaged the same transect from the coast to the Brazilian craton. Together these data result in a seismic transect from the Pacific Ocean to the Brazilian craton with a length of more than 800 km.

[11] Field parameters of the near-vertical reflection profiling were especially designed to image the deep lithosphere. Sections imaging the uppermost crust in some parts of the section were available through industrial contributions by Empresa Nacional del Petróleo (ENAP) (Chile) in the offshore shelf area and the Longitudinal Valley and by Yacimientos Petroliferos Fiscales Bolivianos (YPFB) (Bolivia) in the Altiplano. Therefore near-vertical profiling in this survey was performed with a relatively wide shot spacing of 6 km. Each shot was fired twice off-end into 252 recording channels at 100 m spacing resulting in a 50-km-long split spread when the spread had completely moved. The resulting nominal subsurface coverage was fourfold. The shots were fired in 20-m-deep boreholes with 90 kg explosive charges; five holes in Bolivia were fired with 300 kg charges.

[12] From 10 locations along the ANCORP transect, repeated shots were fired into the 25-km-long geophone line in order to achieve seismic observations at large offsets. The wide-angle measurements, mainly for velocity control, were integrated in this program by repeating these shots up to 9 times with increasing charges (up to 450 kg) after each complete move up of the recording spread. Of these wide-angle shot points, one was 6 km offshore, operated by the Chilean Navy, and one was at the mine Quebrada Blanca using regular quarry blasts (40 t charges). The resulting shot sections reach maximum registration offsets of 120 to 230 km.

[13] Recording was done by 56 independently operating three- and six-channel Teledyne PDAS stations with strings of six geophones of 4.5 Hz natural frequency (sampling interval of 10 ms). Subsequent seismological monitoring of local and teleseismic earthquakes was completed in March 1997 after a 3-month continuous operation by a wide-spread stationary network consisting of 30 PDAS-recording stations (Figure 1) [*Haberland and Rietbrock*, 2001].

4. Reflection Seismology

4.1. Data Processing

[14] The first processing of the ANCORP near-vertical incidence data set [*ANCORP Working Group*, 1999] focused on the image of the down going slab and did not fully exhaust the scientific potential of the data. The aim of extensive reprocessing was a higher resolved image of the entire crustal structure with particular emphasis on already observed spectacular events, such as the Nazca Reflector and Quebrada Blanca Bright Spot [*ANCORP Working Group*, 1999]. The details of the processing sequence are found in Appendix A (section A1). Processing results with a low-fold common depth point (CDP) stack section and a finite difference poststack depth migration based on the wide-angle velocity model are depicted in Foldouts 1 and 2.

[15] Despite the processing efforts, several disadvantages and problems were not or incompletely solved during processing. These include aspects like insufficient spatial sampling due to large geophone spacing; the absence of proper static corrections due to a lack of closely spaced near-surface measurements; the inability to allow normal moveout (NMO) velocity analyses and an improvement of signal-to-noise ratio during stacking because of the low CDP fold; and the control of the generally high noise level (air blast, earthquakes, electromagnetic interspersions). In summary, these restrictions are assumed to be responsible for not allowing producing a phase-true high-resolution zero-offset stack. Other important aspects, like the effects of strong lateral CDP scattering caused by severe deviations of the profile from a straight 2-D line and significant altitude variations along the profile were tested by an additional migration approach to check the validity of the 2-D approach. A Kirchhoff prestack depth migration was performed in 3-D from topography using the true shot and receiver locations and avoiding elevation-related static corrections (see Foldout 2c).

4.2. Results

4.2.1. Main Reflective Features

[16] ANCORP was surveyed only with wide-spaced explosive sources focusing mainly on the deep structures. Therefore the uppermost 5–10 km are not well resolved due to the relatively high shot point interval of about 6.3 km. Although shot quality varied along the profile, the explosive charge of 90 kg in combination with maximum source-receiver offsets of 25 km generally was high enough to achieve penetration depths down to 100 km as shown by energy decay curves from single shot traces. The migrated final seismic reflection result and the automatic line drawing (Foldouts 1 and 2b) show a number of prominent features described as follows.

[17] An east dipping ($\sim$20°) reflection band connected to the subducting Nazca plate [*ANCORP Working Group*, 1999] is clearly visible beneath the Coastal Cordillera, the Longitudinal Valley, and the Precordillera, namely, from profile km 0 at a depth of 50 km in a laterally coherent manner down to a depth of more than 80 km at profile km 110, where it gradually disappears. Above and parallel to it, there is a thick reflective zone starting at 30 km depth at profile km 0 down to 40 km depth at profile km 30. It continues more diffusely between depths of 45 km at profile km 55 down to a depth of 55 km at profile km 105 where it ends. Also parallel to, but below the main Nazca reflection, discontinuous reflections are present, e.g., at 55 km depth at profile km 0, at 65 km depth at profile km 25, at 70 km depth at profile km 50, and at 80 km depth at profile km 80. Compared to the poststack result, the prestack image of the Nazca reflection band is better resolved into two parallel reflectors (Foldout 2c) starting at 40 km and 50 km, respectively. The Nazca Reflector (NR) itself appears more focused over most of its extent and can be followed down to depths greater than 80 km. The prestack image also indicates a prolongation of the NR below 80 km depth. However, due to the relatively strong reflectivity of the QBBS and its rather complicated internal structure the image of the NR below it appears weaker and blurred. Although there is little doubt about the existence of such a prolongation, the image here itself does not allow a qualitative estimate of reflectivity.

[18] The event with the highest amplitudes within the section is the so-called Quebrada Blanca Bright Spot [*ANCORP Working group*, 1999]. It dips west ($\sim$20°) beneath the Precordillera from a depth of 25 km at profile km 170 to a depth of 35 km at profile km 125. At its eastern end it splits up into 3 to 4 single reflections. Diffraction-like events have been successfully removed during migration.

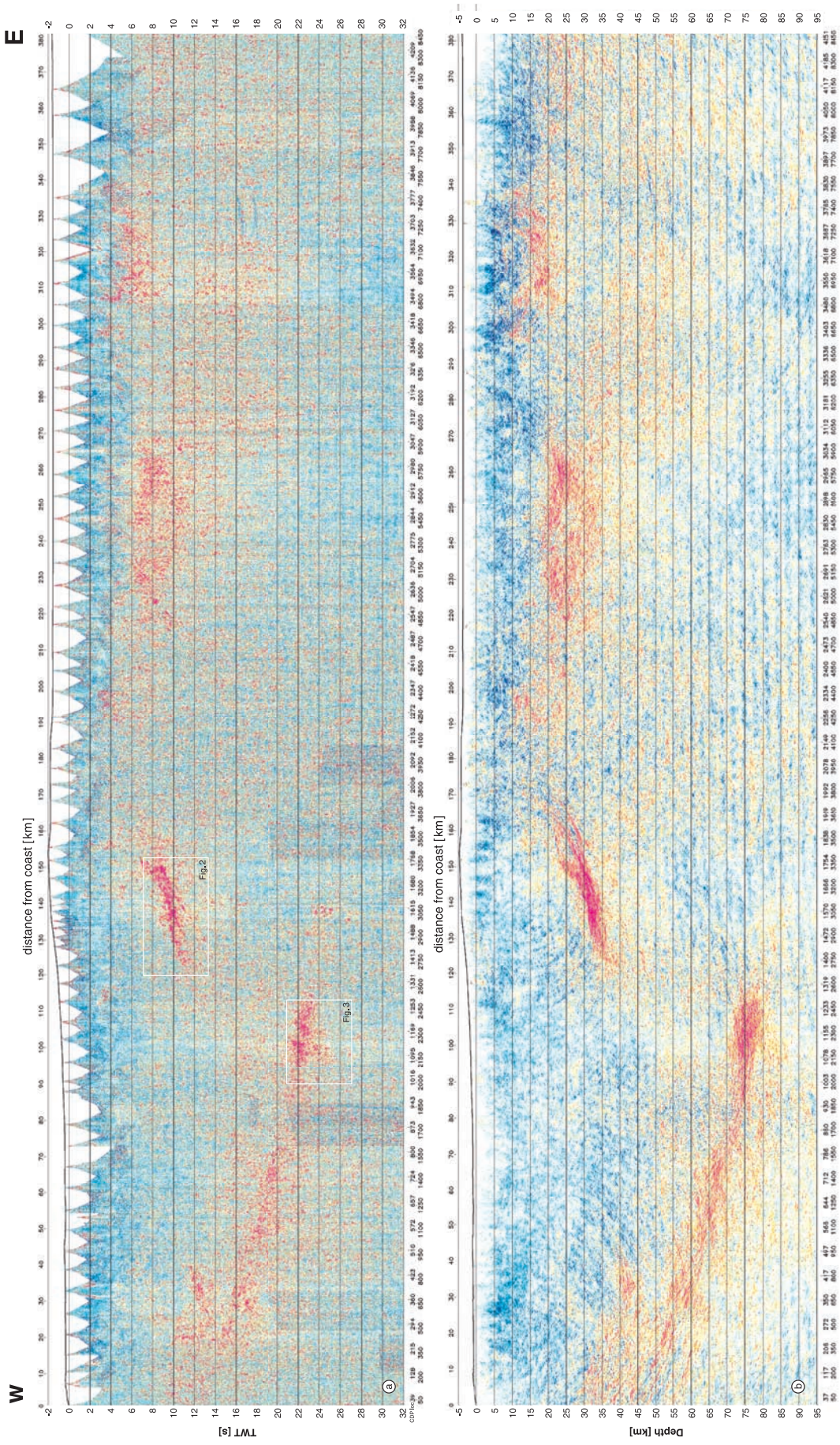

Foldout 1. (a) CDP stack (about sixfold coverage) of the ANCORP 96 reflection line. TWT zero corresponds to sea level, yielding negative times for the mountain ranges. White rectangles indicate details shown in Figures 2 and 3. (b) Poststack depth migration of the CDP stack. The color code is such that large amplitudes are shown in red (positive) and yellow (negative), whereas small amplitudes are shown in blue (positive) and green (negative), respectively. See Appendix A for processing details. See enlarged version of this figure in the HTML.

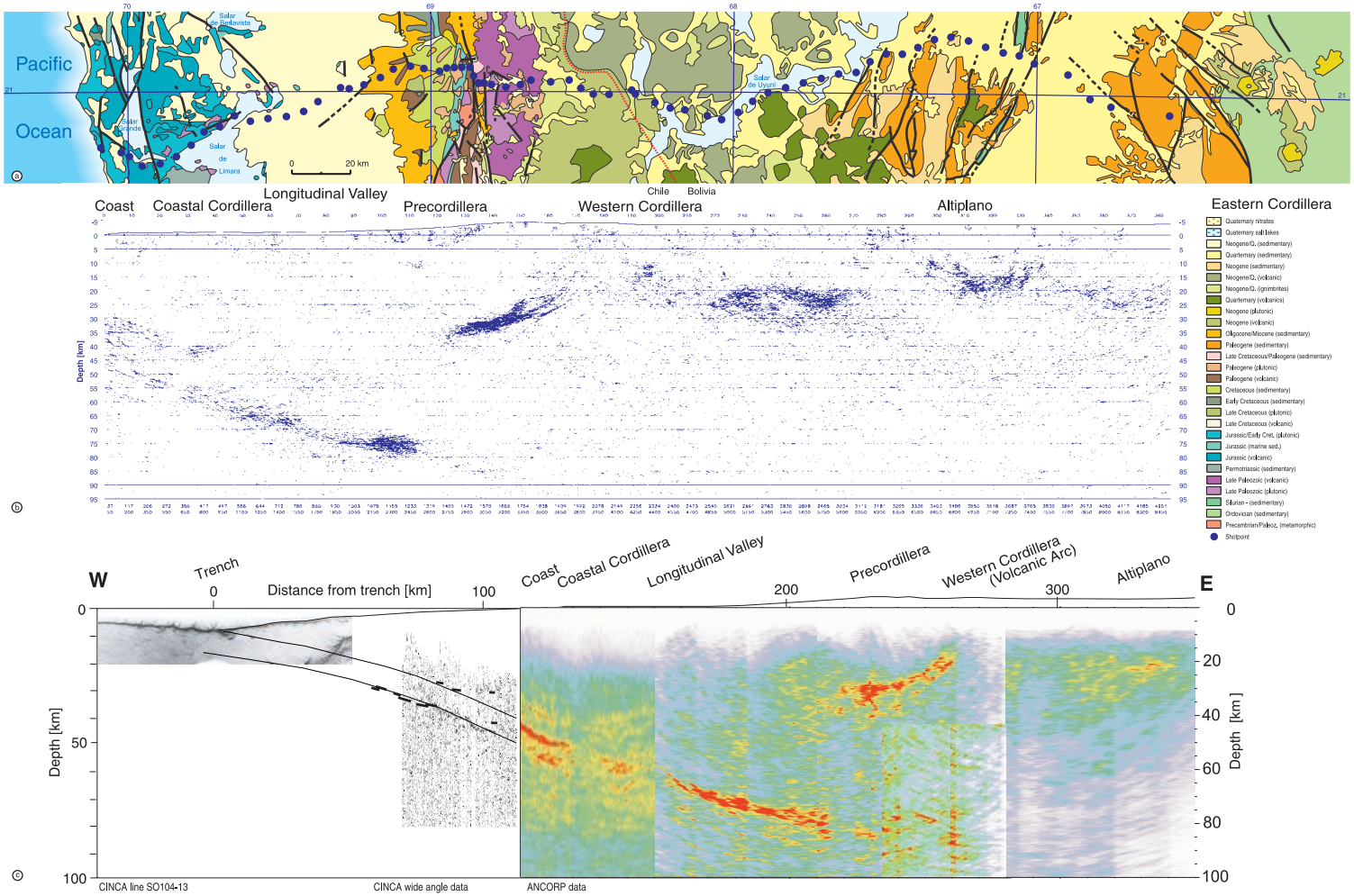

Foldout 2. (a) Geological strip map of ANCORP transect [from *Reutter et al.*, 1994]. (b) Automatic line drawing of the migrated section in Foldout 1b. Only laterally coherent phases are enhanced, and random noise is rejected. (c) Prestack Kirchhoff depth migration of the forearc portion of the ANCORP profile, extended offshore by the stacked wide-angle results of the CINCA experiment, and by the migrated wide-angle CMP reflections (black bars) [see *Patzwahl et al.*, 1999], as well as by the reprocessed CINCA multichannel line SO104-13 [*Buske et al.*, 2002]. Thin lines indicate location of oceanic crust from the CINCA velocity model (see Figure 5). Between 40 km and 50 km depth the Nazca Reflector consists of two sharply imaged parallel reflectors that continue downdip. Below the Quebrada Blanca Bright Spot a more diffusive prolongation of the Nazca Reflector appears at depths greater than 80 km (see text for discussion). See enlarged version of this figure in HTML.

Moreover, from images computed perpendicular to the profile orientation from the prestack 3-D-migrated data it also becomes clear that the QBBS is not a simple north-south striking element but dips slightly to the north.

[19] Two other, more than 10 km thick reflective bodies are visible beneath the Altiplano, one at a depth from18 to 33 km at profile km 218 to 275, the other at a depth of 13 to 24 km at profile km 310 to 335. Two more diffuse smaller reflective bodies are observed at a depth of 15 to 20 km at profile km 195 and at a depth of 25 km at profile km 365. Below the Altiplano the overall reflectivity shows a general decrease at a depth of 60 to 70 km between profile km 170 and 385. All other events, especially those with a bowl-like shape are to be interpreted with care since they might be migration artifacts generated by singular high amplitudes or at the ends of strong reflections.

4.2.2. Details of Key Structures

[20] The specific characters of the entire section are the strongly reflecting domains, none of which can be directly linked with a well-known surface feature. In order to better constrain interpretation, two of three main features of the ANCORP section, the Quebrada Blanca Bright Spot (QBBS) and the dipping Nazca Reflector (NR), have been analyzed separately. This analysis was directed at providing additional information about their internal structure and reflectivity including the question of reflection polarity. The INDEPTH group has employed a similar strategy to study the polarity of the controversially discussed Nyinzhong Bright Spot in Tibet [*Brown et al.*, 1996; *Makovsky and Klemperer*, 1999]. This feature, however, was much more pronounced and coherent in comparison to our QBBS. The procedure devised for this polarity-preserving data processing is described in more detail in Appendix A (section A2).

[21] Two shots fired at the same position (peg 1643) located directly above the QBBS have been merged together to a single record section yielding a 50-km-long split-spread configuration and have been processed as described in Appendix A. Figure 2 shows the west dipping band of high reflectivity of the QBBS (strong color) as a display area filled by a color code according to the instantaneous amplitude. It is apparently constituted of discontinuous events with a sequence of positive and negative phases of various spacing, possibly indicating bodies or layers of different acoustic impedance with varying thickness (Figures 2c and 2d). In some regions, the first ''reflections'' are more pronounced (left part). In others there is a high continuous reflectivity caused by some internal structure, possibly accompanied by some internal multiples (right part). At several places, the reflective band clearly starts with a negative polarity (first coherent phase is blue, Figure 2e), at others it seems to start with a positive polarity (first coherent phase is red, Figure 2f). In summary, there is no unique indication for a negative polarity at the top of the reflective zone, although a simple statistical evaluation (picking and counting of the first coherent phases) shows that about two thirds of the QBBS first phases are blue (i.e., negative polarity). An analogous evaluation for the lower boundary of the QBBS reflective zone (picking and counting of the last coherent phases) resulted, however, in more or less equally distributed portions of positive and negative polarities.

[22] A similar test was performed for the Nazca reflector merging two shot gathers from shots at the same position (peg 1140) located directly above the deepest visible part of the NR to a single record section and processing it as described above (Figure 3). The contrasts between low reflectivity and higher reflectivity are not as pronounced as for the QBBS. However, the east dipping coherency is recognizable including also some unexpected smaller domains of west dipping reflectivity. The statistical method of picking and counting the first and last coherent phases yielded an equal distribution of positive and negative polarities for both the upper and the lower boundary of the NR band. While these observations do not allow a statement concerning the polarity as well as the absolute value of reflection coefficients for the Nazca Reflector zone, this analysis hints at an internal structure of the NR with domains of conflicting dips that were not observed in the conventionally processed data.

5. Refraction and Wide-Angle Data

5.1. Data Processing and Modeling

[23] The wide-angle data set consists of 10 shot sections composed of 70 single shot registrations of ~25 km length each. The sections reach maximum registration offsets of 120 to 230 km. They are on average shorter than the seismic refraction profiles measured in previous campaigns in the study area [*Wigger et al.*, 1994; *Patzwahl et al.*, 1999; *Schmitz et al.*, 1999],but the high shot point density (on average one shot per 35–50 km) allows for a much better resolution of lateral variations in the velocity model. The data coverage along the transect is represented by the first break travel time curves for all wide-angle shot sections (Figure 4c). Details of the processing procedure are found in Appendix A (section A3).

5.2. Results

[24] Four sections highlight the most important results. The section of shot point 1 (Figure 4a) actually consists of two parts. The near offsets (0–75 km) were observed using borehole shots at the Pacific coast and only the far offsets (70–230 km) were observed using offshore shots. As this part of the section contains the most important information about the crustal structure we concentrate on this part. Three different phases can be identified in the section. The *Pg* phase is observed as a very clear onset over the whole length of the section with a nearly constant apparent velocity of 6 km/s and a reduced (by 6 km/s) travel time of 0–0.5 s. The next phase is labeled as *PmP*(c). It is observed from 140 to 180 km offset at 4 to 3.5 s reduced travel time. This phase is the dominating late phase in the section. The second late phase in the section (*PmP*(o)) has weaker amplitudes and can be clearly observed only along a relatively short part. From about 140 km offset the onsets of this phase are interfered by a long coda of the *PmP*(c) phase. Clear observation of this phase is possible from 120 to 140 offset and between 7 and 6.5 s reduced travel time.

[25] The section of shot point 4 (Figure 4a) spans nearly 300 km of the profile from the Coastal Cordillera until the western Altiplano plateau. The part of the section observed westward mainly confirms the relatively constant velocity of the *Pg* phase also observed in section 1. Turning to the east, the section suggests a strong lateral heterogeneity of the velocity distribution of the crustal part covered by our

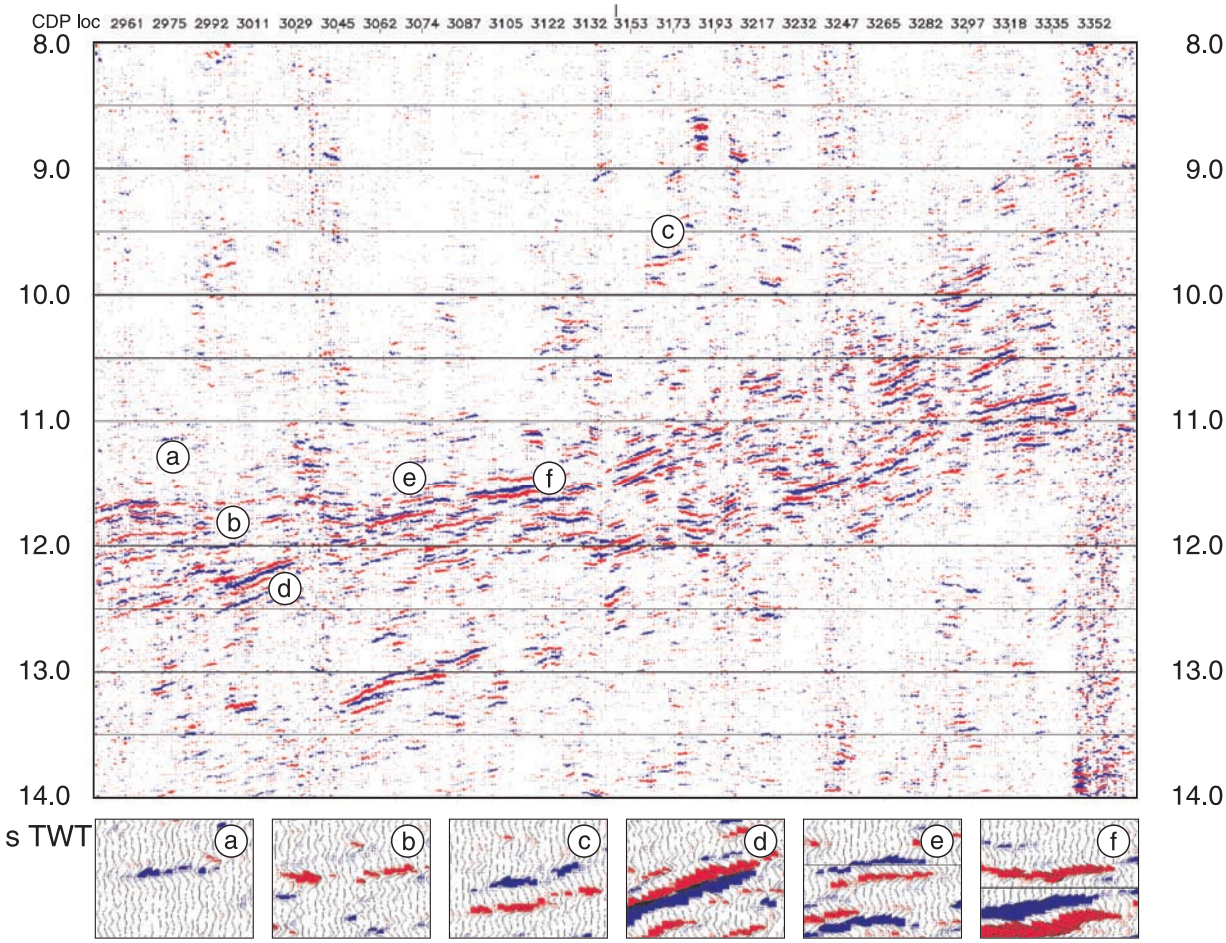

Figure 2. Single shot section after phase-preserving deconvolution showing the Quebrada Blanca Bright Spot region complemented by several enlargements Figures 2a–2f), i.e., (a) single positive reflection; (b) single negative reflection; (c) and (d) reflection sequences from layers of different thickness; (e) first reflection is positive; and (f) first reflection is negative. See Foldout 1 for location of enlargement.

observations. Although observations up to 170 km offset from shot point 4 are available, the *Pg* phase can only be traced until about 95 km offset. There, fading of the amplitudes of the *Pg* phase suggests a velocity inversion at about 10 km depth. The phase that is dominant from 100 to 140 km offset is labeled *Pgl*; this phase resulted from diving and turning below the velocity inversion. The thickness of the inferred low-velocity layer is about 5 km. From 140 to 160 km offset, there is only extremely weak energy to be observed with no clear onsets, which may imply strong heterogeneities in the upper continental crust of the Western Cordillera and Altiplano.

[26] The sections of shot points 6 and 8 (Figure 4b) contain observations from the Altiplano domain. Here it is obvious that the amplitudes of the *Pg* phase fade out, and, at about 0.5 s reduced travel time later, the *Pgl* phase (diving wave from below a velocity inversion at about 10 to 15 km depth) becomes the dominant phase of the section.

[27] From these sections, several results can be summarized for the velocity structure of the entire margin system (Figure 5a). The forearc region between the Pacific coast and the volcanic front has already been described as seismically relatively fast based on earlier investigations [*Wigger et al.*, 1994; *Schmitz and Kley*, 1997; *Patzwahl et al.*, 1999; *Schmitz et al.*, 1999]. A north-south running profile at the coastline revealed only a thin layer with *P* wave velocities below 6 km/s. From 5 km depth to about 20 km depths, velocities range between 6.4 and 7.0 km/s [*Wigger et al.*, 1994]. A refractor interpreted as the Moho refractor by *Wigger et al.* [1994] is located at 40 to 45 km depth below the profile. The low-velocity zones between 20 and 30 km and 35 and 40 km were not resolved by the east-west profiles of the transect at 21°S and are not included in the E-W velocity model. Modeling of the *Pg* phases of the ANCORP wide-angle data from the forearc reveals a velocity of more than 6.0 km/s already at shallow depth (0 to 2 km). Down to 20 km depth velocities increase to 6.5 km/s with a decreasing trend toward the east. Down to about 50 km depth underneath the Longitudinal Valley *P* wave velocity increases to ~7 km/s, constrained by the *PmP*(c) phase in the refraction data. Wide-angle phases from that depth were also observed in an earlier experiment by *Patzwahl et al.* [1999] and corroborate a weakly east dipping base of the forearc crust at some 50 km depth. The phase *PmP*(c) correlated in the sea shot has its reflection points at 50 to 55 km depth below the Longitudinal Valley

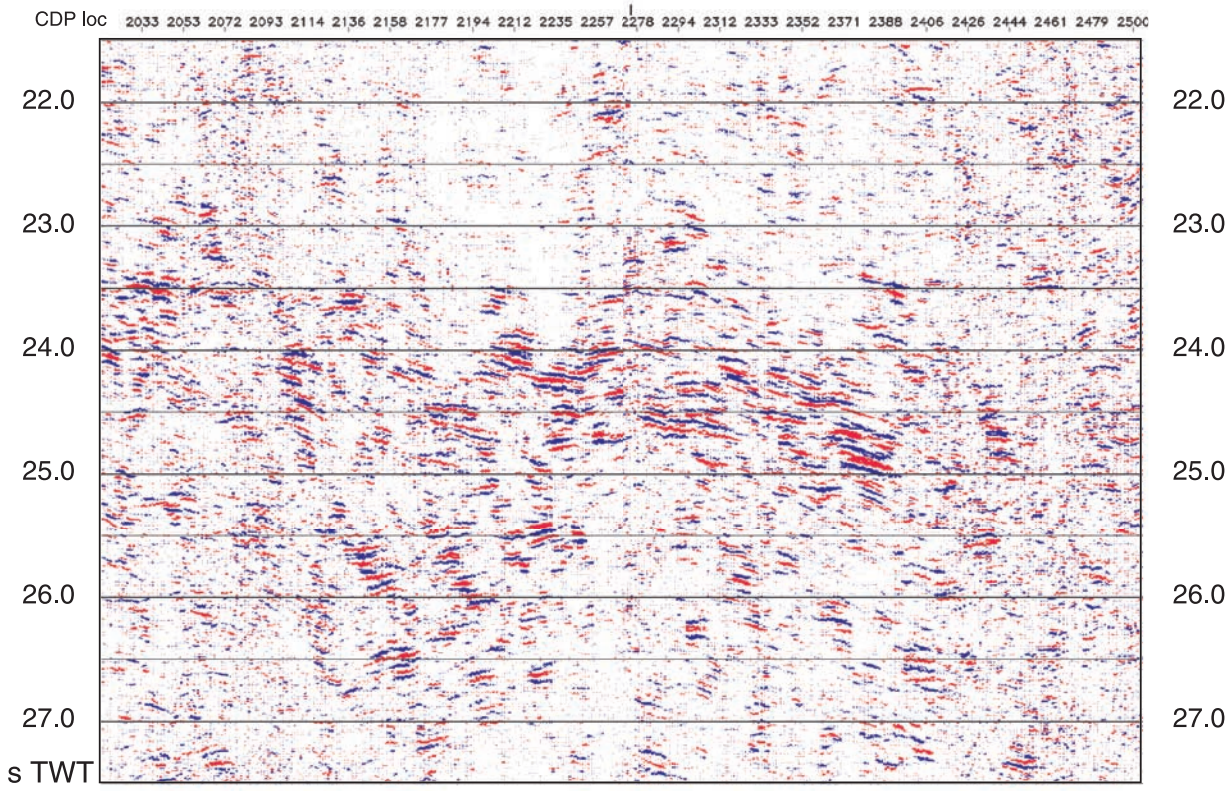

Figure 3. Single shot section after phase-preserving deconvolution showing the Nazca Reflector in more detail. Note contrasting dips in upper and lower part of the reflector band. See Foldout 1 for location of enlargement.

with a dip of about 11° toward the east. The reflection points of this phase are well above the upper border of the Nazca Reflector, which is here at 60 to 70 km depth. The reflection points of the *PmP*(o) phase are at about 55 km depth beneath the western part of the Coastal Cordillera. This is the depth at which the discontinuous reflector below the Nazca Reflector is imaged suggesting its coincidence with the oceanic Moho.

[28] The recent arc region comprises the Western Cordillera and the western part of the Bolivian Altiplano. The crust of the arc is generally slower than that of the forearc [*Wigger et al.*, 1994; *Schmitz et al.*, 1999]. A low-velocity layer with a velocity reduction of ~1 km/s begins in the arc region at 15 km depth. This low-velocity layer can be traced into the Bolivian back arc by seismic refraction data as well as by analysis of *P-S* converted waves [*Yuan et al.*, 2000]. The crustal thickness at the western margin of the arc region is constrained by N-S seismic refraction profiles [*Schmitz et al.*, 1999]. A Moho depth of 65 to 70 km has been inferred. A continental wide-angle Moho underneath the Bolivian Altiplano has not been observed.

[29] Analysis of a long distance refraction profile [*Wigger et al.*, 1994; *Schmitz and Kley*, 1997; *Patzwahl et al.*, 1999; *Schmitz et al.*, 1999] revealed a crustal thickness of roughly 70 km underneath the Eastern Cordillera as indicated by a Moho reflection registered from a shot point near Tupiza in the Eastern Cordillera. The reversed shot at Ollague did not reveal any Moho reflection underneath the Altiplano. Intracrustal wide-angle reflections on that shot as well as correlation on the sections measured during the ANCORP campaign across the Altiplano indicate a thick low-velocity layer with velocities between 4.0 and 5.8 km/s in the first 15 km below the surface. Below this layer, velocities are between 6.0 and 6.4 km/s at about 20 km. Velocities below were not resolved by ANCORP wide-angle registrations despite of up to 160 km maximum offset on the Altiplano. The critical distance of a 70-km-deep Moho would have been at roughly 160 km offset as had been shown by registrations of the shot point Tupiza [*Wigger et al.*, 1994]. Whereas wide-angle investigations on the Altiplano were not able to detect a crust-mantle discontinuity, receiver function investigations found a Moho at some 60–70 km depth underneath the Altiplano [*Yuan et al.*, 2000, 2002].

6. Correlation Between Geophysical and Geological Data

6.1. Correlation of Seismic Data With Other Geophysical Data

[30] Below the Coastal Cordillera, earlier wide-angle data from a N-S running section by *Wigger et al.* [1994] and receiver function analysis of teleseismic events by *Yuan et al.* [2000, 2002] indicate that an inferred continental Moho is located at some 40 km depth (Figure 6b). While we do not observe wide-angle reflections at this position in our E-W section, a bundle of strong, near vertical incidence reflections between 25 and 40 km depth is observed above this depth that rises to the west in the

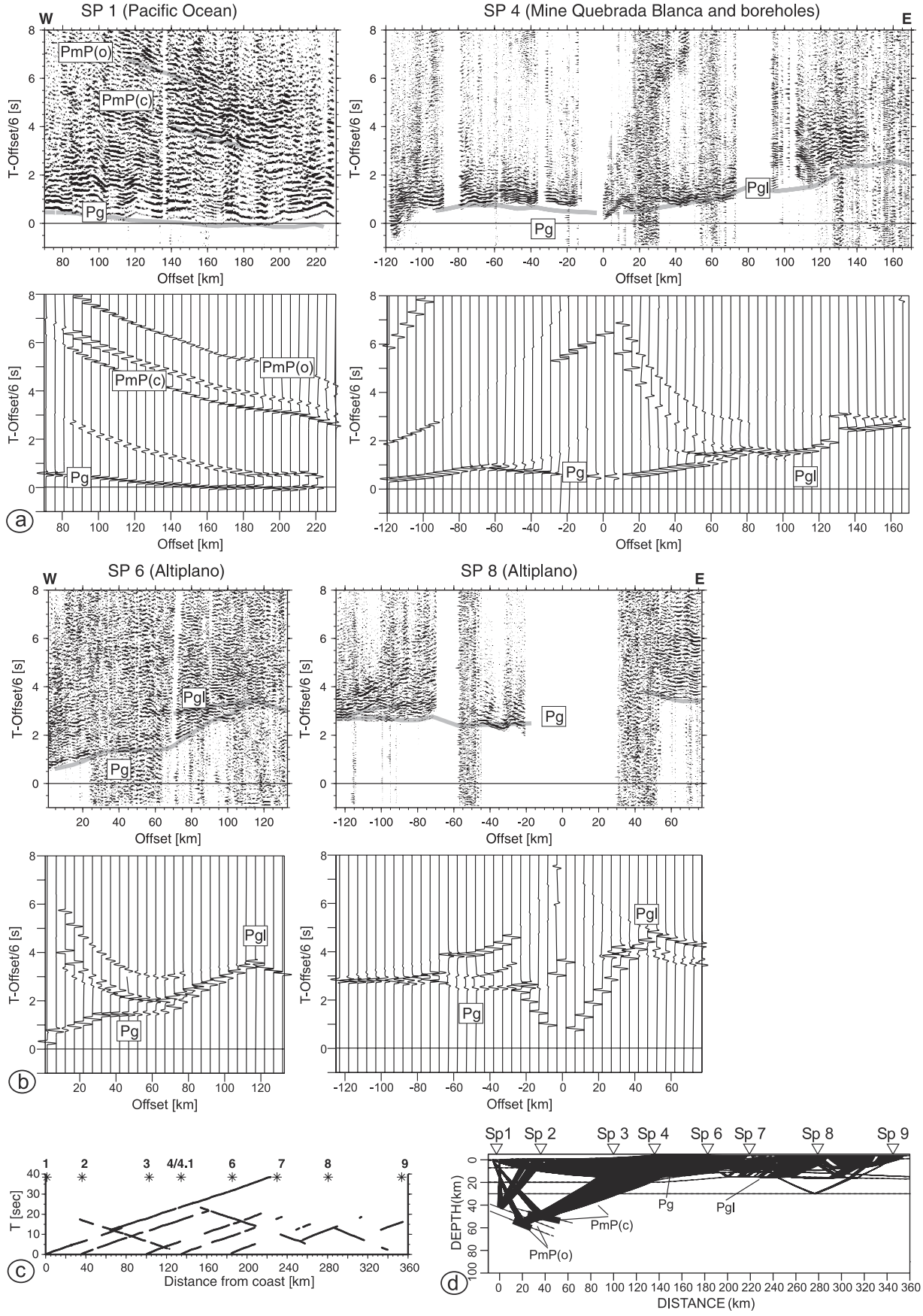
W
SP 1 (Pacific Ocean)
SP 4 (Mine Quebrada Blanca and boreholes)
E
PmP(o)
PmP(c)
Pg
Pgl
T-Offset/6 [s]
Offset [km]
a
SP 6 (Altiplano)
SP 8 (Altiplano)
b
1
2
3
4/4.1
6
7
8
9
T [sec]
Distance from coast [km]
c
Sp1
Sp 2
Sp 3
Sp 4
Sp 6
Sp 7
Sp 8
Sp 9
DEPTH(km)
DISTANCE (km)
d

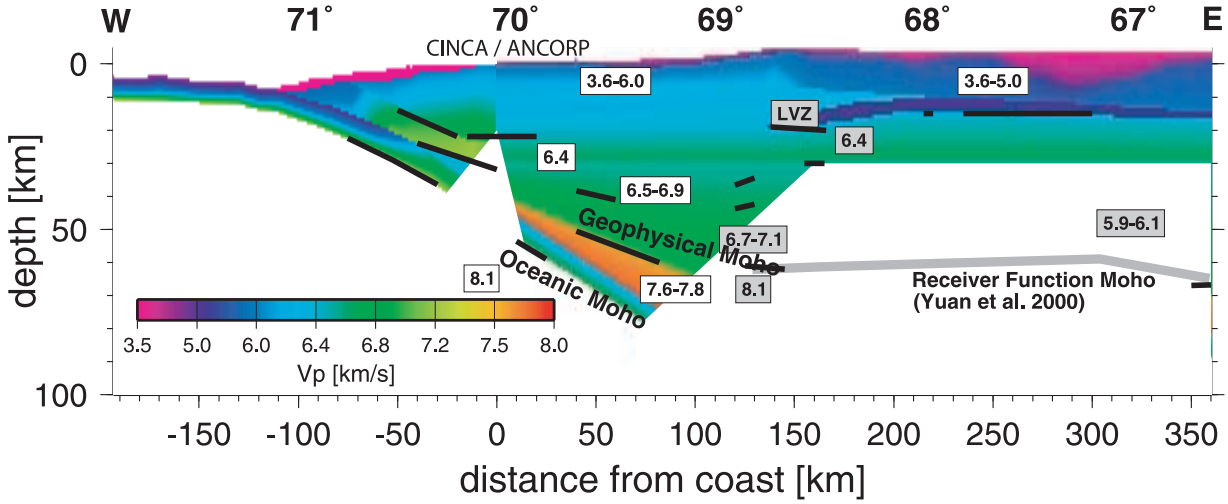

Figure 5. Velocity model as derived from seismic refraction and wide-angle registrations along the ANCORP transect extended by offshore velocity model obtained during the CINCA experiment [*Patzwahl et al.*, 1999]. Velocity values (V_p) in white boxes are the velocity ranges of the respective layers. Velocity values (V_p) in grey boxes are from seismic refraction measurements from earlier experiments [*Wigger et al.*, 1994; *Schmitz et al.*, 1999; *Patzwahl et al.*, 1999]. The color-coded area indicates the part of the model that is covered by phase correlations in the wide-angle sections. Thick black lines denote reflector elements. The reflector elements from below the western and eastern plateau margin are from *Wigger et al.* [1994]. The grey line at 65-75 km below the plateau is the Moho position as inferred from receiver function data [*Yuan et al.*, 2000].

otherwise transparent forearc crust. In the offshore domain, the top of this feature is continued by a westward rising wide-angle reflection that indicates a downward velocity increase to some 7.2 km/s [*Patzwahl et al.*, 1999]. A few km above the western end of this feature, the crust is topped by a thin low-velocity layer, that can be linked to a thin sedimentary cover (< 1 km) observed in the reflection sections of the marine CINCA'95 survey [*CINCA Working Group*, 1999]. This cover is strongly deformed by normal faults and, toward the trench, is increasingly collapsed and slumped [*Von Huene et al.*, 1999].

[31] Farther east below the onshore forearc, weak reflectivity at 50–55 km depth beneath the Longitudinal Valley can be seen to be related to a wide-angle reflection and a modeled downward increase of velocity of ~7 km/s to ~7.6 km/s (Figure 6b). Toward the east, below the Precordillera, an earlier experiment by *Wigger et al.* [1994] had shown another wide-angle reflection at some 65 km depth, interpreted by them as the Moho reflection. While the vertical incidence reflection data show no further correlating reflection events with the inferred wide-angle forearc Moho, the receiver function data [*Yuan et al.*, 2000] suggest a strong positive velocity contrast at the recorded depths although the velocities below the convertor may be lower than standard mantle velocities (Figure 6c).

[32] Below the Nazca Reflector the receiver function analysis has identified another convertor with a positive velocity contrast toward depth [*Yuan et al.*, 2000] (Figure 6c). This event correlates with the discontinuous single reflections observed to parallel the Nazca Reflector some 6–8 km deeper. The Nazca Reflector and the parallel deeper reflection are both continued in the data from the offshore CINCA'95 reflection and wide-angle experiment, the shots of which were also recorded on land (Foldout 2c). Modeling of these wide-angle data and migration of the wide-angle CMP reflections by *Patzwahl et al.* [1999] clearly shows that a deeper velocity boundary can be directly linked to the reflection and convertor below the Nazca Reflector. This deeper velocity boundary continues toward the oceanic realm where it links with a near vertical incidence reflection at some 6–8 km below the surface of the oceanic plate interpreted by the *CINCA Working Group* [1999] as the oceanic Moho. The Nazca Reflector was shown by *Patzwahl et al.* [1999] to be linked to a low-

Figure 4. (opposite) (a) Data and synthetic seismograms of shot point 1 (in Pacific Ocean) and shot point 4 (quarry blasts of Quebrada Blanca Mine and borehole shots) in the Precordillera. The data have been band-pass-filtered 2–16 Hz and reduced with 6 km/s reduction velocity. Modeled travel time curves of the correlated phases are indicated by grey lines. The travel time curves and the synthetic seismograms have been computed using the velocity model described in Figure 5. Travel times and amplitudes have been determined with a ray theoretical code [*Zelt and Smith*, 1992]. (b) Data and synthetic sections of shot points 6 and 8 (on the Bolivian Altiplano). Processing and details as in Figure 4a. (c) Travel time diagram indicating the coverage of refraction/wide-angle reflection recordings. The travel time curves of the direct *P* wave (*Pg* and *Pgl* phases) are shown for all shot points. (d) Ray diagram showing the ray paths of all correlated phases of all shot points. The reflection points of the *PmP*(o) (oceanic Moho) and the *PmP*(c) (Moho of the continental crust) phases are indicated by black lines at 60 and 45 km depth, respectively.

velocity channel underlying the offshore forearc up to the trench where its reaches the surface of the crust. We interpret this feature and the Nazca Reflector to indicate the plate interface. This interpretation is also supported by the teleseismic receiver function study by *Yuan et al.* [2000] who have observed a double convertor between 60 and 120 km depth, interpreted as an image of the oceanic crust. The upper convertor, likely imaging the upper boundary of the

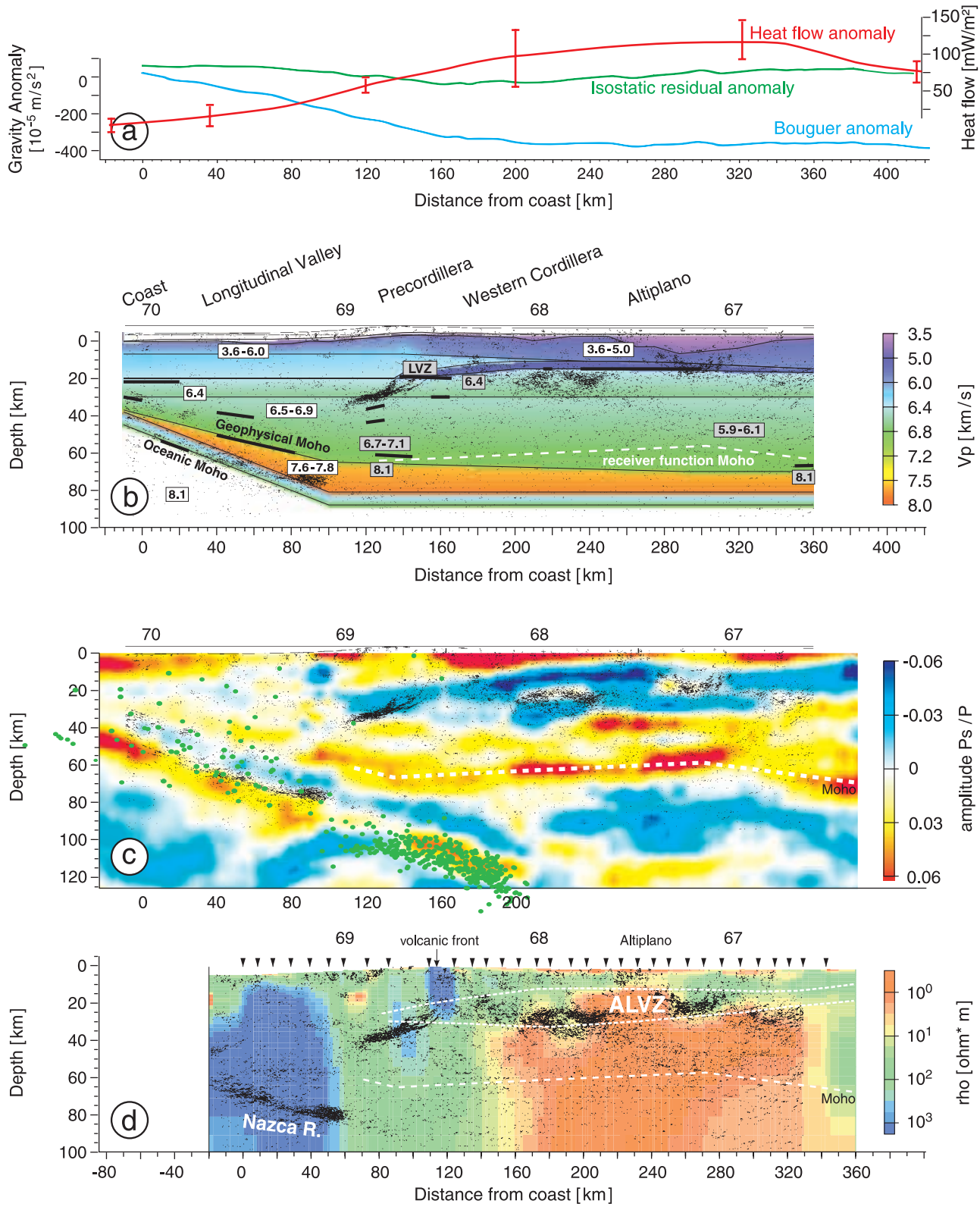

subducting oceanic crust, nearly exactly coincides with the Nazca Reflector.

[33] Seismicity, as recorded during the passive seismological experiment along with earlier data from the global data set, shows a more complex relationship to the Nazca Reflector (see *ANCORP Working Group* [1999] for details). In the upper domain, above some 60 km depth, seismicity scatters widely about the Nazca Reflector and does not indicate a well-defined seismic coupling zone between both plates (Figure 3c). The intermediate-depth seismicity below 60 km shows a very complex pattern in the central Andes. While a clear double seismic zone with an average offset of 20–25 km can be observed to the north of our study area (Arica region) [*Comte et al.*, 1999], there is no equivalent observation in the Antofagasta region [*Graeber and Asch*, 1999]. Between 80 and 120 km depth, a conspicuous, 25-km-wide band of intermediate depth seismicity is offset from the downdip end of the Nazca Reflector toward depth by some 10–20 km where it continues with the same dip. The positive polarity seismic convertor (*S* velocity increase downward) observed in both teleseismic [*Yuan et al.*, 2000] and local [*Bock et al.*, 2002] receiver function data at this depth transects the seismicity cluster and links with the sharp reflector below the Nazca Reflector. Both are interpreted as the oceanic Moho. Accordingly, the 25-km-wide band of intermediate depth seismicity is only partly localized in the oceanic crust (observed thickness of some 6–8 km), and some must occur in the oceanic mantle. Note, however, that most of the receiver function data have been collected some 100–400 km to the south of the ANCORP line.

[34] The petrophysical nature of the Quebrada Blanca Bright Spot remains complex [*ANCORP Working Group*, 1999]. The laminated strong reflections are located below a low-velocity zone (maximum depth at some 20 km) in the wide-angle data detected by earlier wide-angle observations from the shot point Ollague at the Chilean-Bolivian border [*Wigger et al.*, 1994, cf. also *Schmitz et al.*, 1999]. The reflections, however, precisely relate to a strong *P*-to-*S* convertor, clearly visible in all data including sparse data from the ANCORP network, that indicates a downward velocity decrease at the site of the reflections [*Yuan et al.*, 2000] (Figures 6b and 6c). Polarity analysis of the near vertical incidence data also indicates a tendency toward a downward velocity decrease (see above). The strongly laminated aspect of the bright spot (Figure 2), however, also suggests that a layering between "higher" and "lower"-velocity or density zones with respective thickness of several hundred of meters and lateral extent of up to several kilometers may be present. A feature of this dimension may well be "visible" in near vertical incidence data, and also show up as a convertor, but may not necessarily be resolved in wide-angle observations. Finally, the bright spot area neither shows up as an anomaly in gravity data [*Goetze and Kirchner*, 1997; *Romanyuk et al.*, 1999], nor in magnetotelluric depth soundings [*Brasse et al.,* 2001] (see Figures 6a, 6b, and 6d). Subsequent 3-D modeling of the latter data by *Lezaeta* [2001], however, has shown that a zone of moderately low resistivities (in the order of some tens of ohm meters) with the size of the Quebrada Blanca Bright Spot may well be present and compatible with the data.

[35] Some of these observations are repeated in the Altiplano area. Wide-angle registrations across the Altiplano have revealed low velocities between 4.0 and 5.8 km/s in the first 15 km that are not easily correlated with the reflection data due to restricted near surface resolution of the ANCORP data. Industry reflection data clearly show a folded thick stack of partly exposed Phanerozoic sediments to a depth of at least 4 s two-way time (TWT) [*Baby et al.*, 1997]. Velocities below 15 km are poorly constrained by wide-angle registrations. However, several other experiments such as receiver function analysis [*Yuan et al.*, 2000, 2002], surface wave tomography [*Vdovin et al.*, 1999], and local earthquake tomography [*Myers et al.*, 1998; *Haberland and Rietbrock*, 2001] revealed anomalously low average velocities throughout a depth range of about 60–70 km. This observation has been reported to be the crustal thickness underneath the Altiplano [*Isacks*, 1988; *Beck et al.*, 1996; *Swenson et al.*, 2000; *van der Lee et al.*, 2001], where it correlates with the observed decay of reflectivity.

[36] Receiver function analysis [*Yuan et al.*, 2000], and the above tomographic analysis, has identified an important low-velocity zone across the entire Altiplano at around 10–40 km depth. The near vertical incidence data show patches of considerably increased reflectivity at the same depth level (15 to 35 km depth below surface), which again is below the depth of resolution of the ANCORP wide-angle data. Earlier wide-angle observations by *Wigger et al.* [1994] from the shot point near Ollague toward the east were also interpreted with a LVZ between 10 and 20 km depth below the western Altiplano. Thus the upper boundary of the western Altiplano reflectors at about 15 km would again coincide with a refractor below a LVZ, as found for the Quebrada Blanca bright spot, while the internal velocity distribution of the bright patches is again unresolved. Also, V_p-V_s tomography indicates that the entire middle and deep crust of the Altiplano is characterized by V_p-V_s ratios well above 1.78 [*Schurr et al.*, 1999; *Schurr*, 2000; *Yuan et al.*, 2000, 2002].

[37] Moreover, the entire Altiplano crust east of the volcanic arc below some 20 km was found to be extremely conductive with resistivities as low as 1 Ω m in contrast to the forearc area (Figure 7d) [cf. *Brasse et al.*, 2002]. This model was achieved by two-dimensional inversion of a

Figure 6. (opposite) Correlation of reflection results with other geophysical data. (a) Gravity and heat flow data along the ANCORP section (see *Goetze and Kirchner* [1997], *Romanyuk et al.* [1999], and *Springer* [1999] for details). (b) Wide-angle results superposed on automatic line drawing of ANCORP results. (c) Receiver function data [*Yuan et al.*, 2000] superposed on automatic line drawing of ANCORP results. Green dots are seismicity projected from a maximum distance of 0.5° into the section and located using the average velocities obtained from the ANCORP wide-angle component. (d) Electrical resistivity model [*Brasse et al.*, 2002; *Schwalenberg et al.*, 2002] superposed on automatic line drawing of ANCORP results along with Altiplano low-velocity zone (ALVZ) and Moho trace from receiver function data [*Yuan et al.*, 2000]. Note that the lower boundary of the Altiplano conductor is poorly resolved.

long-period magnetotelluric data set (10-10,000 s). With this procedure the inherent problem of static shift of apparent resistivities was at least partly overcome by employing mainly the magnetotelluric (MT) phases. Although the lower boundary of the Altiplano conductor is not resolved, two-dimensional sensitivity studies and exploration of model space by *Schwalenberg et al.* [2002] imply a minimum thickness of 20 km and an integrated conductivity (conductivity-thickness product) of 20,000 S for this structure. Also, while no conductor was modeled for the Nazca Reflector, a conductor above the subducted Nazca Plate at ~60–90 km depth (perhaps imaging devolatization reactions) may well be compatible with the data set if the a priori model used as the starting model is changed accordingly.

[38] A heat flow density profile along 21°S shows low heat flow density at 20–30 mW/m^2 (data in Figure 6a and interpretation in Figure 7b are based on work by *Springer* [1999] and *Babeyko et al.* [2002]) in the forearc, rising to 40–60 mW/m^2 in the Precordillera. The Western Cordillera and Altiplano are characterized by large variations of heat flow density between 50 and 180 mW/m^2, which decreases eastward to about 50–80 mW/m^2 in the Eastern Cordillera and to about 40 mW/m^2 in the sub-Andean zone and the Chaco. A 2-D subduction model with conductive heat transfer assuming steady state adequately describes the forearc temperature field [*Springer*, 1999]. Because of partial melting and potential convective heat transfer in the Altiplano-Puna region 2-D thermomechanical modeling has been applied [*Babeyko et al.*, 2002]. The models explain the midcrustal low-velocity and high-conductivity zone as well as the high and strongly variable surface heat flow as due to convective bulk flow of the deeper crust at high basal beat flow from the mantle (> 60 mW/m^2) during tectonic shortening.

6.2. Correlation With Surface Geology

[39] Of the features described above, only those in the upper 30 km of the crust can be seen to have a more or less distinct link with, or expression in, geological and topographic surface features (Foldout 2a). The offshore low-velocity layer at the top of the crust correlates with the sediment cover of Neogene age. The latter covers the forearc crust of mostly Jurassic age along a subaerial unconformity in grabens and half grabens that are related to syndepositional subsidence. On land, this kinematic regime, now associated with uplift, continues up to the Atacama fault system, which marks the transition into the Longitudinal Valley. The outcrop trace of this subvertical fault system precisely overlies the eastern end of the reflective forearc lower crust. The entire unit overlying the reflective high-velocity deep crust is built from a magmatic arc developed during Jurassic times on Paleozoic continental crust [*Rutland*, 1971]. Related magmatism was shown to have a predominantly mafic character [*Haschke et al.*, 2002].

[40] The Quebrada Blanca bright spot further east underlies the Precordillera at the western margin of the Altiplano. At surface its boundaries are clearly linked to two first-order features, the subvertical Precordilleran fault system in the west and the recent volcanic front in the east (active since 13 Ma [*Baker and Francis*, 1978]). The area above this bright spot is characterized by the worlds largest concentration of porphyry copper mineralizations most of which were formed during the Paleogene. Structural analysis shows that the Precordilleran fault system, that was probably used as a conduit for mineralizing fluids, was initiated as a transpressional strike slip fault in the core of the Paleogene magmatic arc at around 35–40 Ma [e.g., *Reutter et al.*, 1996]. Recent kinematics involves low strain rate dextral transtensional strike slip motion along steeply dipping faults. These are partly associated to a strong magnetotelluric anomaly reaching as deep as the forearc mantle [*Brasse et al.*, 2002] (compare Figure 6d). Although the upper crustal architecture differs markedly across the fault (thin Meso-Cenozoic cover on Paleozoic basement in the east versus thick cover of the same age in the west), no substantial change in geophysical properties is observed across the fault apart from the reflection bright spot. In summary, the features limiting the bright spot are presently active and are related to fluid or melt transport.

[41] The midcrustal reflective domains below the Altiplano east of the Quebrada Blanca bright spot show another relationship to the surface geology. While there is no conspicuous correlation with single structures, their regional subsurface extent matches the extent of Miocene volcanism at surface. This was shown to also hold in a more regional perspective for the observation of a midcrustal *P*-to-*S* convertor across the entire plateau between ~20° and 26°S [*Yuan et al.*, 2000]. Findings by *Trumbull et al.* [1999] from the Altiplano-Puna volcanic complex corroborate this relationship with magmatism. Although the latter is situated slightly further south (24°), the lateral continuity of the receiver function image supports extrapolation of these data to the ANCORP line. There, the isotope signature of Miocene and younger ignimbrites indicates melt formation above the depth of garnet stability (~30 km) and below the depth of plagioclase fractionation (20 km). This depth range again correlates with the position of the reflective patches. Moreover, the dominant feature known from the surface of the southern Altiplano, the Uyuni-Kenayani transpressional fault system [*Baby et al.*, 1997; *Lamb et al.*, 1997], that was active during the Miocene, can be seen to link with dipping reflections that merge into the above midcrustal reflection domains. Structural interpretation of industry seismic sections further north [*Lamb and Hoke*, 1997] and near 21°S [*Baby et al.*, 1997] indicates flattening of the steep near-surface structures in the Altiplano area at a depth of some 12–15 km in agreement with the observed flattening of the Uyuni-Kenayani fault system (see above and Figure 7b). Accordingly, these large plateau-crossing structures would seem to be either older than the midcrustal reflective features or, more likely, they sole out into these features. The weak, moderately west dipping reflection fabric in the deeper crust (below 30 km depth east of 68°) cannot be linked to surface features and rather indicates a separation of upper and lower crustal reflectivity-forming processes.

7. Discussion

7.1. The Crust-Mantle Boundary

[42] In contrast to "standard" Moho images of orogenic belts, the Andes show a variety of Moho features that may help to identify stages in the evolution of the crust-mantle

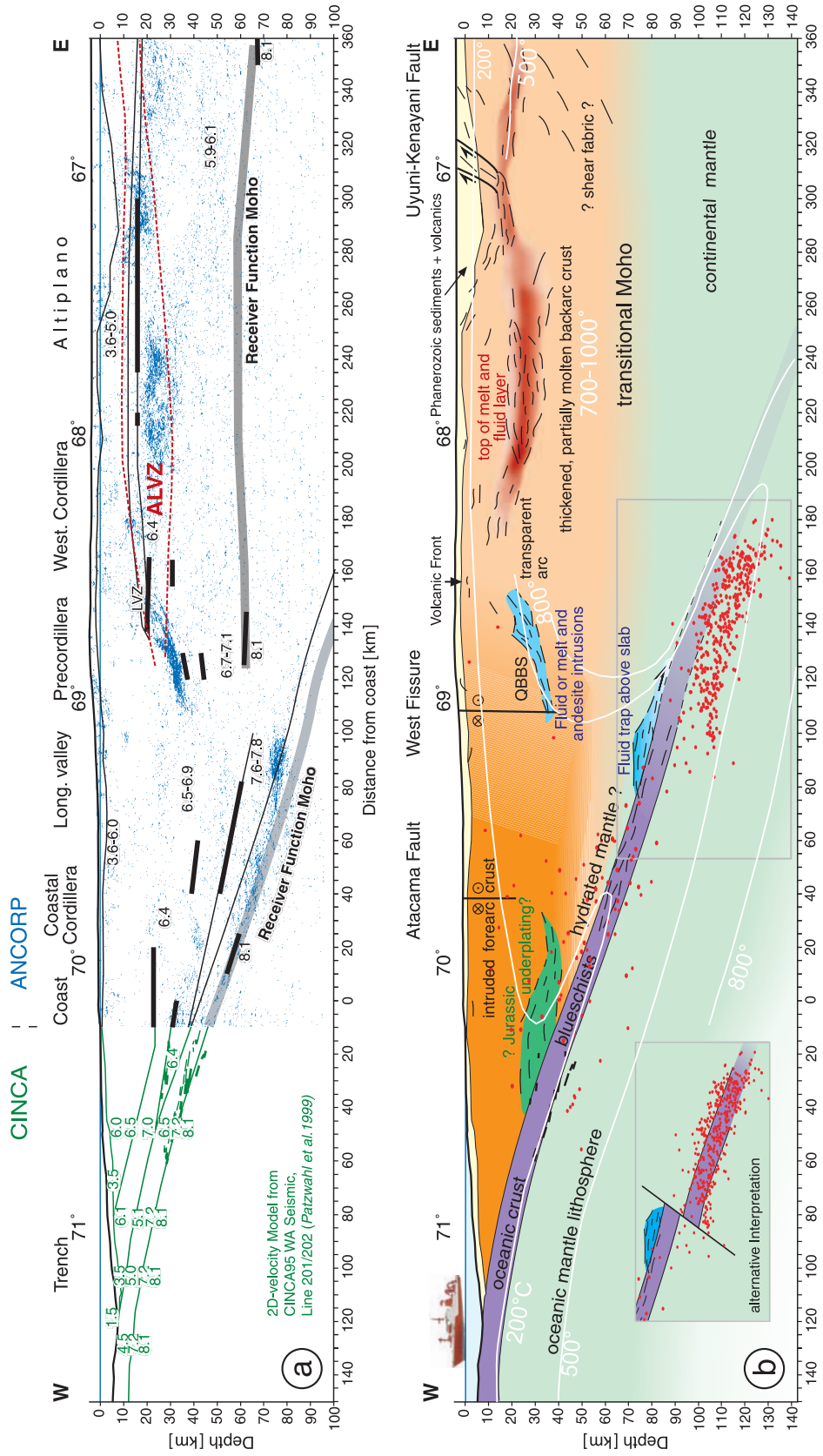

Figure 7. Seismic results and interpretation. (a) Automatic line drawing of depth-migrated ANCORP reflection data, including onshore wide-angle and receiver function results [*Yuan et al.*, 2000], merged with results from the offshore CINCA experiment and its onshore recording [*Patzwahl et al.*, 1999]. (b) Suggested interpretation of seismic observations including an alternative interpretation of the relation between slab geometry and seismicity. Isotherms from *Springer* [1999] are only included for the forearc due to unconstrained convective heat transfer below the plateau. See text for details.

boundary during orogeny and the parameters controlling this evolution [*Giese et al.*, 1999]. Four domains can be identified that show different Moho images: the down going oceanic Nazca plate, the continental forearc, the plateau, and the Brazilian shield.

[43] Offshore wide-angle data and reprocessed offshore multichannel data (see *ANCORP Research Group* [1999], *Patzwahl et al.* [1999], and *Buske et al.* [2002] for details) link the Nazca Reflector with the top of the oceanic crust and subduction shear zone, and the parallel sharp, weaker reflector some 6–8 km deeper with the oceanic Moho (Foldout 2c and Figures 5 and 7a). While the oceanic reflection Moho can be followed in segments down to about 85 km, near the updip end of the intermediate depth seismicity cluster, its image in receiver function data south of 23°S is still visible to 120 km at the downdip end of intermediate depth seismicity [*Yuan et al.*, 2000]. The reflection fade out at some 85 km corresponds to the lower stability limit of amphibole minerals in mafic rocks [*Pawley and Holloway*, 1993] suggesting a domain of active eclogitization and fluid release in this depth range. Accordingly, the downdip continuation of the receiver function image of the oceanic crust below 85 km was suggested to indicate kinetically delayed eclogitization of the down going slab [*Yuan et al.*, 2000]. Hence the change in oceanic Moho aspect below 85 km and its complete disappearance at some 120 km are taken as evidence for prograde metamorphism of basaltic material in the descending slab [see *Yuan et al.*, 2000]. The progressive downdip change of frequency-dependent imaging characteristics of the oceanic crust may also indicate that metamorphism is related to a progressively more complex geometry of the reaction front.

[44] In the continental forearc domain, the mantle wedge between the Nazca Reflector and the continental Moho, as inferred from wide-angle data and converted phases from teleseismic data, appears to be more reflective than the overlying continental crust. The forearc mantle from this interpretation has lower than average mantle velocities (7.6 km/s) and a high V_p/V_s ratio with values between 1.75 and 1.83. This joint observation is here suggested to indicate heterogeneously hydrated mantle above the down going slab [cf. *Peacock*, 1997]. The appearance of a Moho signal in converted phases, which employ low-frequency/long-wavelength signals with a lower resolution capacity, in contrast to a lacking short period reflection image, can be seen to indicate a transitional base of the crust with a width of several kilometers. The latter is probably related to the hydration process and its geometry.

[45] At the base of the magmatic cordillera and back-arc area below the thickened Altiplano crust a reflection and wide-angle Moho are again nowhere observed with exception of wide-angle reflections from some 65–70 km depth from beneath the Precordillera and the Eastern Cordillera [*Wigger et al.*, 1994; *Schmitz and Kley*, 1997]. Some single shot gathers and the stack section show a broad zone of diminishing reflectivity in the back-arc area in the 50–80 km depth range. The mantle properties below 70–80 km vary substantially across the entire system as evidenced from travel time tomography, Q tomography, and mapping of the V_p/V_s ratio [*Schurr*, 2000; *Haberland and Rietbrock*, 2001]. Temperature modeling by *Springer* [1999] indicates that Moho temperatures below the plateau are consistently above 800°C, in places exceeding 1000°C. At these conditions, even largely dehydrated and refractory crust may show minor grain boundary melts that are sufficient to explain the velocity properties, high V_p/V_s ratio, high attenuation, and high conductivity. The lateral continuity of these petrophysical properties in the crust above the inferred Moho across the entire plateau would suggest that the processes affecting the crust-mantle boundary image are the same across the entire arc and back-arc area. Also, recent observations on the *S* wave velocity structure from the upper mantle beneath South America by *van der Lee et al.* [2001] showing low velocities down to 150 km depth below the plateau have been suggested to indicate slab-derived fluids (~0.15 wt %) and related partial melts.

[46] Although the ANCORP experiment terminates at the Eastern Cordillera, earlier data indicate a change of the Moho image at depth. The "cold" eastern margin of the plateau under the Eastern Cordillera [*Springer*, 1999] again has a well-defined wide-angle Moho [*Wigger et al.*, 1994; *Schmitz and Kley*, 1997] that precisely correlates with the receiver function Moho at some 65 km depth [*Yuan et al.*, 2000; *Swenson et al.*, 2000]. Under the eastern flank of the eastern Cordillera, reprocessing of industry reflection data by *Allmendinger and Zapata* [2000] indicated that the Moho was not imaged by these data but must be below a depth of 41 km. Toward the east below the foreland, the receiver function data by *Yuan et al.* [2000] and *Swenson et al.* [2000] indicate a rise of the Moho to some 30 km depth.

[47] In summary, the combined image at the crust-mantle boundary across the Andes is probably due to active processes which mask a sharp crust-mantle boundary like hydration of mantle rocks (in the cooler parts of the forearc system), magmatic underplating and intraplating under and into the lowermost crust, partial melting, etc. in the actively heated parts of the system (arc and back arc). As a result, the central Andes show either a broad crust-mantle transition rather than a well-defined Moho or the active processes occurring at the Moho level generate structures with scaling properties that are not susceptible to controlled source methods with a short period signal. In both cases, this is probably an expression of active fluid-assisted metamorphic and magmatic processes at high temperatures occurring in the crust-mantle transition zone.

7.2. Nature of the Major Reflectors

7.2.1. Nazca Reflector and Wadati Benioff Zone

[48] The Nazca Reflector, overlying the lower bound of the reflection and conversion oceanic Moho is probably located within the interplate shear zone as inferred from the distance to the interpreted Moho image. In its shallow part (45–55 km) near the coast, the reflector has a relatively simple structure and moderate strength, which is consistent with the lithological boundary between ultramafic mantle and oceanic crust with some tectonic mélange. However, this interpretation cannot be applied to the deeper part of the reflector, which has a complicated (layered) structure, large strength, and controversial polarity. We suggest that three major processes contribute to the strong reflectivity in the interplate shear zone in

this part. These are (1) massive dehydration of oceanic crust (near upper Amphibole stability limit) supplying fluids into the shear zone, (2) formation of hydrous phases like serpentine and possibly also talc [*Peacock and Hyndman*, 1999] in the mantle and within the shear zone accompanied by volume increase and destruction of permeability, thus resulting in trapping of fluids at the mantle hydration front, and (3) slab-parallel shearing of the weak hydrated mantle containing trapped fluid-rich lenses or pockets. While the first two processes tend to produce a highly variable, incoherent seismic impedance pattern with locally very high impedance contrasts, the third process tends to produce coherent structures aligned downdip that are capable of producing seismic reflections with a Fresnel zone of several km. The *ANCORP Working Group* [1999] suggested that the source of the fluids is related to massive dehydration at the lower limit of amphibole stability within the down going oceanic crust. In order to produce these reflections by a reaction front as well as by fluid trapping and shearing, the rate of fluid release from the oceanic plate has to be higher than the rate of percolation through the upper plate. The mechanical behavior of such a complex shear zone and particularly the style of interaction between deformation, serpentinization, and fluid porous flow remain unknown.

[49] A consequence of this interpretation is that the Nazca Reflector should disappear or at least lose its strength substantially at a depth where either dehydration of the oceanic crust is largely completed or where temperatures in the forearc mantle become too high for serpentine stability (higher than 650–700°C). According to temperature estimates from surface heat flow in the central Andes [*Springer*, 1999], at least one of these conditions is very likely met at a depth of 80–90 km where the Nazca Reflector does disappear. This suggests an inherently thermal control of reflectivity continuation and breakdown.

[50] Alternatively, the zone of strong reflectivity above the slab may have originated due to shearing of a mantle unit, which was already hydrated heterogeneously some time earlier. In this end–member model no fluid traps are required and the reflections are produced by the boundaries between strongly sheared, seismically anisotropic serpentinites and peridotites. We suggest that in reality both, sheared bodies of previously hydrated mantle and fluids trapped at fronts of ongoing serpentinization contribute to the strong reflectivity observed in the deep portion of the Nazca Reflector.

[51] Intermediate–depth earthquakes from the Wadati–Benioff zone are offset downdip from the Nazca Reflector by some 20 km to below the oceanic reflection Moho and cluster at some 100 km depth below the western Cordillera, the active magmatic arc (Figure 7b). If the slab crust continues linearly downward from the Nazca Reflector, then a major part of this seismicity is located within the oceanic mantle of the Nazca plate [*ANCORP Working Group*, 1999]. This however is in conflict with observations a few degrees to the south of the ANCORP line, where both local source [*Bock et al.*, 2002] and teleseismic [*Yuan et al.*, 2000] receiver function studies report that most of the seismicity at about 100 km depth (the cluster of which is significantly thinner here) is located within the ~8 km thick oceanic crust. The larger width of some 25 km of the cluster at the 21°S latitude, however, requires that a significant part is located in the mantle of either the upper or the lower plate. The width and offset of seismicity at 21°S may be due to local reactivation of some feature within the down going slab (fracture zone, magmatic ridge, etc.) as suggested by *Kirby et al.* [1996] for the deeper seismicity along the same plate boundary. Alternatively, as suggested by *Rietbrock and Haberland* [2001] the Nazca plate may have a tear at the ANCORP line (see inset in Figure 7b). This is consistent with the peculiar curved shape of the earthquake cluster at the ANCORP line, which is specific for this location and is not observed elsewhere in the central Andes.

7.2.2. Quebrada Blanca Bright Spot

[52] Bright spots are often interpreted to be caused by fluids or melts. As mentioned above, however, there is an inconsistency between the extraordinary strong reflectivity of the Quebrada Blanca bright spot, which may indicate the presence of fluid or melt, and the absence of a good conductor in the MT data that precludes the existence of a large body containing interconnected fluid or melt there. If no fluid or melt is involved, some very strong lithological contrast is required to explain the observed reflectivity. Taking into account that the bright spot is located close to or within the magmatic arc, this contrast may be due to a mafic intrusion (or multiple intrusions) into felsic country rock. In order to consider this more quantitatively we have calculated reflection coefficients for the boundary between solidified intrusions of andesitic and gabbroic compositions and country rocks consisting of a felsic rock with a bulk chemical composition as suggested for the average central Andean crust by *Lucassen et al.* [1999]. We employ the modeling technique of *Sobolev and Babeyko* [1994], which combines methods of thermodynamic petrology (direct Gibbs' free energy minimization) and rock mechanics (calculation of mechanical properties of compounds) to calculate equilibrium mineralogical composition, density, and seismic velocities for a rock of an arbitrary bulk chemical composition equilibrated at lithospheric pressures and temperatures. The intrusion is located at a depth of 30 km (lithostatic pressure of 0.85 GPa) at a temperature between 500 and 700°C. The resulting single–boundary reflection coefficients for P (S) waves are close to 0.08 (0.05) for andesitic and to 0.12 (0.09) for gabbroic intrusion. These values may increase to maximum of 0.20 (0.15) in the case of constructive interference if intrusions are multiple. Although we were not able to estimate the reflection coefficient at the QB bright spot in this study, it seems that it may be well above 0.2. Also, polarity analysis has indicated that negative polarity at the upper boundary of single layers dominates over positive polarities. If this is correct, then melts or fluids are still required. They should, however, either form small, localized bodies or a noninterconnected network to be consistent with MT data - which would be in line with the discontinuous reflection image of the QBBS (Figure 2).

7.2.3. Altiplano Reflectors

[53] We believe that the key to understanding the origin of the Altiplano reflectors is their correlation with strong P-to-S conversions, a large electrical conductivity anomaly (Figure 6d), a high V_P-V_s ratio domain, the high surface

heat flow, and the lateral extent of young magmatism of partly crustal origin. All these features suggest that these reflectors mark the top of a partially molten zone in the crust. While our data do not allow a more detailed analysis of the seismic properties of these reflectors with the aim to differentiate between melts and fluids, as for example provided by *Makovsky and Klemperer* [1999] for the Tibetan bright spots, the melt hypothesis in this case appears more in line with observations. Also, deformation structures at surface, like the important Uyuni-Kenayani fault system, apparently root in these reflections supporting their interpretation as a first order boundary of low mechanical strength.

[54] The lateral heterogeneity of the reflections, which seems to correlate with changes in the topography of the top of the conductivity anomaly, may indicate internal deformation and heterogeneity of the partially molten zone as well as a complex interaction of the partial melts with the upper crust. Note that the Fresnel zone of the typical near vertical reflected wave at the depth of 20 km is a few kilometers, and therefore deformation structures with smaller wavelength will largely destroy reflections. Conversely, subhorizontal shearing at a detachment level may support a larger scale continuity and reflection visibility in places, much like it is argued for the Nazca Reflector. Recent thermomechanical modeling [*Babeyko et al.*, 2002] suggests that crustal shortening may result in intensive intracrustal convection which forms a heterogeneous partially molten weak zone in the middle crust similar to what we observe in the Altiplano.

[55] Interestingly, the geophysical image and the interpretation (Figure 7b) of the plateau domain from the ANCORP results are highly similar to recently obtained results from the other major orogenic plateau on Earth, the Tibetan Plateau, as seen in the INDEPTH results [e.g., *Brown et al.*, 1996; *Nelson et al.*, 1996; *Makovsky and Klemperer*, 1999; *Schilling and Partzsch*, 2001]. In the Andean case, the interpretation is strengthened by the observation of widespread volcanism from an at least partly crustal source, that correlates regionally with the extent of the mid crustal convertor along the plateau [cf. *Yuan et al.* 2000] and with the reflections across strike described here. Hence we conclude that orogenic plateau formation may be intimately linked to widespread, midcrustal melting independent of the geodynamic setting and differences in the heat source.

7.3. Crustal Thickening

[56] The wide-angle and near vertical incidence results presented here do not directly constrain the controversially discussed nature of the plateau forming process [see *Isacks*, 1988; *Kley and Monaldi*, 1998; *Allmendinger et al.*, 1997; *Giese et al.*, 1999; *Lamb*, 2000] with exception of some general conclusions. A lateral difference in geophysical properties of the deeper crust is only observed between the forearc area and the arc/back-arc area in terms of average velocity (6.8 versus 6.1 km/s of the back arc) and electrical conductivity. This fact is easily attributed to the evolution of the present forearc setting in a former magmatic arc regime that migrated eastward during the Meso-Cenozoic. Accordingly, the forearc crust was strongly modified by the addition of mantle-derived mafic melts. Since surface deformation in the forearc is very small, the high-velocity crustal keel is probably a result of Meso-Cenozoic magmatic underplating [cf. also *Haschke et al.*, 2002] that has cooled to low temperatures [*Springer*, 1999]. Plateau uplift since the Miocene and the lack of high-velocity material below the entire plateau, in contrast, preclude a more substantial contribution of magmatic underplating here [cf. also *Isacks*, 1988].

[57] The seismic results from the plateau strongly suggest that deformation is partitioned in an upper crustal domain confined at depth by the bright reflection domains and a lower crustal level down to at least the Moho. The intracrustal boundary level was identified by *Yuan et al.* [2000] [see also *Myers et al.*, 1998; *Chmielowski et al.*, 1999] to coincide with a low-velocity zone (termed Altiplano low-velocity zone, ALVZ; Figure 7a). This zone was interpreted as a decoupling zone that partitioned crustal shortening into a largely brittle upper crust domain with structures flattening into this zone and a ductile deep crust. Because of concentration of most upper crustal contraction above a crustal décollement at the eastern margin of the Altiplano plateau [*Allmendinger and Gubbels*, 1996; *Kley and Monaldi*, 1998], flow of the deeper crust under the ALVZ detachment in cross section must be dominantly westward under the plateau. While the basement below the ALVZ was deformed and shortened in an as yet unresolved mode, the weak internal west dipping reflection fabric within the deeper crust of the eastern Altiplano may be a remnant of this westward underthrusting and stacking of originally more eastward crustal units. Alternatively, it may be indicative of pervasive shearing. The discrepancy between observed and here corroborated crustal thickness and crustal shortening observed from surface structures remains an unresolved problem that probably requires analysis beyond a 2-D perspective.

8. Conclusions

[58] 1. The CINCA and ANCORP experiments imaged the subduction of the Nazca plate beneath the central Andes from the trench to more than 80 km depth beneath the margin of the Altiplano with the deepest so far acquired reflections from an active convergent plate boundary. Toward depth, the Nazca Reflector is slightly offset above the Wadati-Benioff zone along with increasing downdip reflection intensity before gradual decrease below 85 km. The Nazca Reflector is interpreted to be caused by trapped fluids and shearing at the serpentinization front above the dehydrating oceanic slab. This part also shows seismicity that may be attributed to dehydration embrittlement. The oceanic Moho is seen as a weaker reflection below the Nazca Reflection, the downdip continuation of which as a *P-S* convertor transects the intermediate depth seismicity cluster of the Wadati Benioff zone between 80 and 120 km. Hence a major part of the seismicity is located in the subducting mantle.

[59] 2. A particularly bright west dipping reflection at some 20–30 km depth below the Precordillera (Quebrada Blanca Bright Spot, QBBS) has a reflection coefficient of similar strength as the deeper Nazca Reflector. It is possibly related to the presence of fluids rising through deep reaching faults delimiting the Quebrada Blanca Bright Spot

(QBBS). Patches of coherent reflectivity in the back-arc area occur at the same midcrustal depth (15–30 km). They are associated to a low-velocity zone, a level of P to S conversions of teleseismic waves, high conductivity and high V_p/V_s ratios as well as to Neogene volcanism from midcrustal sources suggesting that this feature is related to partial melting below the entire plateau. Similar findings from the Tibetan Plateau [*Nelson et al.*, 1996] suggest that orogenic plateaus may be very weak systems with the upper crust entirely decoupled from a partially molten middle and lower crust.

[60] 3. A distinct reflection Moho can nowhere be observed at the base of the Andean crust. At its expected depth beneath the forearc, weak reflectivity dips eastward from 45 to 55 km depth. Below the Altiplano, minor reflectivity diminishes down to about 20 s TWT (60–70 km). Wide-angle observations only observe reflections from the Moho beneath the plateau margins at a depth range of 60–70 km. Along with a complete Moho image in low-resolution receiver function data, we interpret these observations as showing a broad transition zone at the crust mantle boundary affected by magmatic and metamorphic processes as well as by a possibly complex internal architecture.

[61] 4. ANCORP'96 is the first seismic section to produce a high resolution, deep image of a convergent continental margin and a related plateau. Most reflectivity is linked to active petrological processes related to ongoing subduction, which involve the release, trapping, or consumption of fluids. This result is in contrast to seismic sections across most fossil mountain belts that usually can be interpreted in terms of structure and lithological contrasts only.

Appendix A

A1. Processing Flow for Reflection Data

[62] Each shot record (entire data set ~33,000 traces) was prepared individually before submitting it to the actual CDP processing. All seismic parameters such as amplitude, frequency, phase, travel time, dip, velocity, and coherency were analyzed and treated separately. Key points of the reprocessing were (1) to perform preprocessing mainly in the source domain, (2) to control the desired result after each single processing step, (3) to analyze spatial and temporal parameter variations with a dense spacing, and (4) to make only restricted use of existing nonseismic data.

A1.1. Data Preparation

[63] After best possible correction of all detected mismatches after a validation of data and geometry with a careful consistency and plausibility check (e.g., comparison of first break times as a function of source receiver offsets) a CDP geometry based on a crooked line design was generated. A CDP trace spacing of 45 m along a smoothly curved reflection line resulted in a 4 to sixfold actual subsurface coverage (Figure 1).

A1.2. Noise Wave Attenuation

[64] After application of a DC removal to correct for the instruments amplifier drift (no filters had been applied in the field except the antialias), bad or partly disturbed traces affected by various source-generated and other noise amplitudes or wave trains were identified through visual inspection of each single shot and treated individually (see Figure A1). A total of 34 earthquake events were detected in the reflection data. Elimination of these "reflection-like" events with a long coda with amplitudes higher than the ones generated by the shot itself required "bottom muting," i.e., zeroing all samples from the first occurrence down to the bottom of the record (Figure A1b). Distinguishing between true reflections and seismological events was generally straightforward: Because of multifold subsurface coverage, the presence of coherent phases at the same TWT and CDP in more than one record was a necessary criterion for a reflection generated by the explosive shots.

[65] Air blast waves from the 90 kg (and higher) shots are visible without any absorption along the entire spread of 25 km and recording length of 60 s (Figure A1a). They were removed by a sharp "surgical muting" (Figure A1b) after a linear moveout (LMO) with the average sonic speed of 335 m/s, zeroing of the now plus/minus horizontally lying wave trains, and reapplying an inverse LMO to retrieve the original time datum. Moreover, the data were contaminated with numerous spikes and singular noise bursts, probably induced by electromagnetic interspersions (Figure A1c). Most of them were detected with an automatic despiking/debursting algorithm by simply comparing the RMS energy of each analysis time window with the average RMS energy of surrounding time windows (i.e., before, behind, and at adjacent traces). The affected time intervals have been zeroed by surgical mutes (Figure A1d).

[66] In near-vertical incidence seismology shear waves and surface waves must be treated as noise that conceals possible reflections. Depending upon their varying strength and character in the different shots, they have been suppressed or eliminated by local frequency filtering, dip filtering, or surgical muting. Classical frequency-wave number filtering failed due to the long recording length and irregular trace spacing along the record.

A1.3. Amplitude Corrections

[67] Taking into account the physical energy decay during wave front propagation a spherical divergence correction via an analytical gain curve has been applied based on an average velocity depth function. In addition, some automatic gain control in the form of a large-window feedback AGC to correct for remaining vertical amplitude level variations was necessary as well as some horizontal trace level equalization based on a crustal-scale time window. Careful parameter selection ensured optimum preservation of the relative amplitude dynamics and also took account of the necessary input assumptions for the following processes.

A1.4. Deconvolution and Frequency Filtering

[68] Traditionally, predictive spiking deconvolution works well with explosive data due to their minimum delay characteristics. For long recording lengths, however, it sometimes fails, since the source signal changes its characteristics along its path, even if multiwindow design is used. Thus a self-updating, so-called adaptive deconvolution [*Griffiths et al.*, 1977] using a maximum entropy algorithm has been applied in forward and reverse direction to remove the effect of the individual seismic source signal from the traces. Deconvolution always involves strong spectral whitening. Hence time- and space-variant zero-phase band-

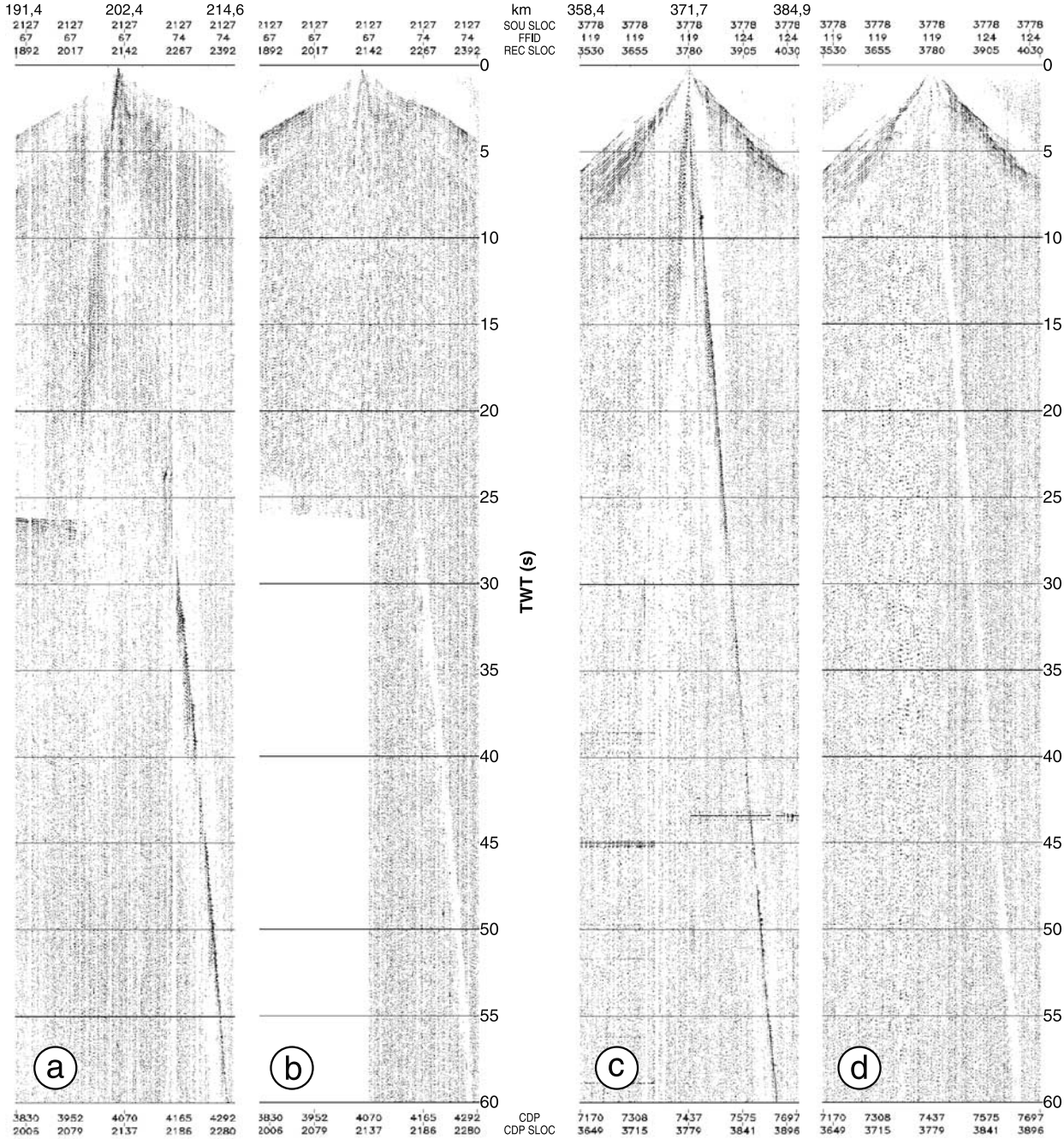

Figure A1. Two raw shot records showing several kinds of severe noise in the data, i.e., (a) earthquake (*P* and *S* arrivals) and air blast wave trains traveling 60 s (more than 20 km) along the receiver line without visible attenuation; (c) spike series probably due to electromagnetic interspersions and air blast wave trains; (b, d) same shot records after adequate suppression or elimination, i.e., bottom mute of earthquake events; surgical mute of air waves; automatic spike detection and replacement by interpolated samples. Horizontal scaling (CDP locations and kilometer scale) corresponds to scaling of seismic section in Foldout 1. See Appendix A for a more detailed description.

pass filters were determined and applied to restrict the amplitude spectra according to the pure signal frequencies that, on average, lie between 5 and 40 Hz.

A1.5. Static Time Corrections

[69] No additional measurements for resolving the near-surface conditions (like accompanying short-refraction lines) had been carried out in the field, since varying velocity and thickness of weathering layers were expected to be no major problem. Therefore purely elevation-based static time corrections using an average correction velocity were calculated to proceed to a common datum from the actual source and receiver positions. However, time delays remained in the data obviously caused by near-surface low-velocity layers. Automatic determination of residual statics

using cross-correlation methods was not convenient due to the low coverage. Hence, as a workaround, individual time delays were determined in the shot domain by wavelength filtering of the picked first breaks and using the differences of the filtered and unfiltered first breaks as residual static time corrections. As a result, a conspicuous overall increase of lateral continuity of reflection events was achieved, although the derived time shifts are not strictly surface consistent.

[70] Because of the large elevation differences (0–4800 m) the total static correction was split into two portions, a smaller one from the actual elevations to an intermediate, so-called ''floating'' datum (following the smoothed topography) which was applied before normal moveout correction, the other, much larger one from the floating to a fixed datum (sea level) which was applied after CDP stacking. In consequence, stacking velocities along the line therefore are more homogeneous and realistic. As a consequence, the time (or depth) zero in the depicted seismic sections corresponds to sea level and, accordingly, the data at higher elevation have negative times or depths.

A1.6. First Break Removal

[71] First breaks, usually diving refraction events, must be removed just as reflection events in wide-angle distances since they do not follow the hyperbolic reflection formulas. So-called ''top'' mutings, individually analyzed for each shot record before NMO, have been applied zeroing the traces offset dependently from time 0 down to 16 s at maximum offset to allow for constructive stacking of near-vertical reflection events. Top muting has been analyzed and applied a second time after NMO to remove remaining nonstackable far-offset portions.

A1.7. Coherency Enhancement

[72] The Fresnel zones in the ANCORP data are wide enough to allow for dip analysis apertures consisting of a sufficient number of traces. In general, the two important input assumptions for most multichannel processes that sample the data horizontally are (1) equidistant traces and (2) no spatial aliasing in the analysis domain. Therefore, prior to any coherency filter routine a regridding to equal trace spacing in the source domain was performed applying common offset binning and stacking followed by filling in of missing traces and surgical mute zones using a wave field reconstruction technique with limited aperture forward and inverse τ-p transforms. Subsequently, actual event enhancement methods in f-x [*Gulunay*, 1996] and τ-p domain [*Kong et al.*, 1985] have been found to give proper results concerning random noise suppression and lateral, dip-preserving coherency increase. Although application before stack is not very common, it worked very efficiently with the low-fold ANCORP data.

A1.8. Dynamic Time Corrections

[73] Evaluation of stacking velocity analyses turned out to be difficult and ambiguous due to the low CDP coverage. Therefore a v_{rms}-TWT background model was derived from turning ray tomographic inversion of the first-break pickings for the upper time range and from the wide-angle data along the ANCORP line for the lower time range to stabilize the finding of appropriate normal moveout velocity pickings for the reflection data. Nevertheless, the results of the NMO-corrected and phase-corrected stacked zero-offset data remain poor, revealing that the basic stacking requirement was not sufficiently met, i.e., alignment of the reflections with an error less than half the dominant signal wavelength. The reasons are assumed to be scattering errors of the surveyed geometry as well as of the static corrections and the low CDP coverage that does not support a sufficient signal-to-noise improvement during stacking.

A1.9. CDP Stacking

[74] To overcome the unsolvable problem of nonconstructive phase-true stacking, another attempt was pursued. Rather than stacking the phases, the envelopes of the NMO-corrected data were constructed via their Hilbert transforms [*Taner et al.*, 1979], and stacked with a straight mean method thus avoiding destructive superimposition at the expense of resolution. Then, the reconstruction of phase-like data was achieved by the so-called perigram technique [*Gelchinsky*, 1985] removing the unwanted DC component. In addition, an attempt was made to restore the amplitude spectra characteristics as they were before envelope construction by applying a spectral shaping process, i.e., scaling of all frequency components to a specified contour and assuming zero-phase relationship. The result is a zero-offset section with similar frequency content as before stacking which, due to its oscillating character, is now migratable (in contrast to the envelope stack) based on constructive and destructive interference (see Foldout 1a).

A1.10. Poststack Wave Equation Depth Migration

[75] In general, automatic migration is difficult to handle in deep seismics, when migration operators become very large (in the order of tens of kilometers) for greater depths at high velocities. As a result, considerable smiles in the lower parts of the sections are created since the basic assumption (noise-free, true-amplitude zero-offset input section) usually does not apply. Several wave equation migration methods such as frequency-wave number, finite differences, and Kirchhoff summation schemes have therefore been tested in time and depth domain to obtain a spatially ''true'' image of the subsurface showing all reflections with the correct dip at the correct depth. A finite differences depth approach using explicit FD extrapolators [*Soubaras*, 1996] with a smoothed interval velocity depth model calculated from the v_{rms}-TWT field turned out to be the best compromise between clear and robust imaging and minimal ''smile''-like artifacts down to depths of 100 km (see Foldout 1b).

[76] For the automatic line drawing of the final result of the ANCORP section (Foldout 2b) an algorithm based on semblance weighting of locally τ-p transformed sliding data subsets has been selected to obtain an appropriate restriction to the imaging of the most important features including the correct handling of conflicting dips if present.

A2. Polarity Analysis

[77] Polarity analysis of the reflections of the bright features (Quebrada Blanca bright spot and Nazca reflection) was carried out in a more extended way as published earlier by *Brown et al.* [1996] for the INDEPTH reflection data. The basic requirement for such an investigation is to retain the original amplitude and phase characteristics for the reflections through all applied processes. Therefore only unstacked traces were analyzed, in practice single good shots are most suitable. Each process that changes the amplitude and phase characteristics is avoided to still

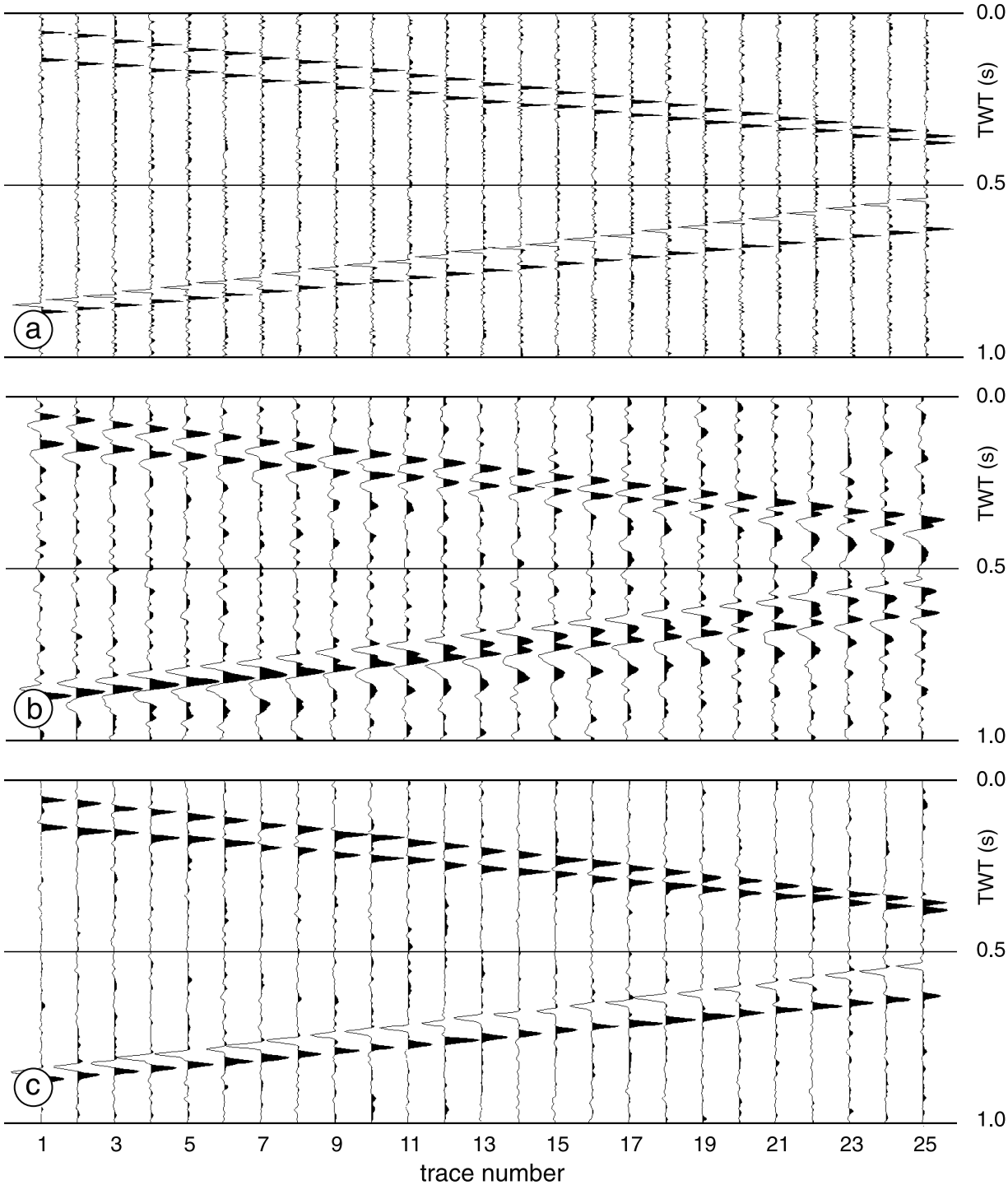

Figure A2. Synthetic section showing two dipping layers with variable thickness and different signs, i.e., (a) reflection coefficients with additive random noise; (b) convolution of the reflection series with a source wavelet derived from ANCORP amplitude spectra; and (c) minimum delay predictive deconvolution yields the correct sign of the original reflection coefficients. Processing is based on single-trace deconvolution and is therefore independent from trace spacing.

allow evaluation of reflection strength and polarity along the trace. The shot impulse is supposed to be a minimum delay signal, which means that it is zero for times less than 0, and of finite duration with its energy maximally concentrated at its front. The first process applied here is a predictive deconvolution (Wiener-Levinson type) to reduce the length of the shot signal down to half a wavelength, which allows better resolution of closely spaced reflections. The design window for determining the deconvolution operator is centered on the reflection band to be analyzed. If the input fulfills the required minimum delay characteristics, then the applied inverse operator is correct

and the output can directly be taken as a pseudoreflectivity series. A subsequently applied minimum-phase band-pass filter will preserve the polarity as well as static and dynamic time corrections. After a horizontal normalizing followed by a moderate time domain coherency enhancement to suppress random noise and to emphasize correlating phases, the single shots are ready for an interpretation of the reflectivity. No absolute reflection coefficients can be derived, but relative ones within the analyzed time window.

[78] A test on synthetic data has been performed to ensure that this procedure works as described. Figure A2a shows two dipping layers, represented by their reflection coefficients, with a thickness changing from several wavelengths down to one sample rate. Also some percent of random noise has been added. Figure A2b shows the same situation for this reflectivity convolved with a (minimum delay) source wavelet that was derived from averaged amplitude spectra of a crustal-scale time window taken from a reflective part of an ANCORP shot. Figure A2c is the result after application of a minimum delay predictive deconvolution without explicit knowledge of the basic source wavelet. Nevertheless, it is clearly visible that the reflectivity has been reconstructed and the phases have been preserved, yielding phase-true pseudoreflection coefficients. The images in Figures 2 and 3 have been achieved by following this phase-retaining processing sequence.

A3. Processing of Refraction Data

[79] The processing of the wide-angle data included (1) editing-removal of bad traces, correction of clock time errors, (2) frequency analysis and band-pass filtering, (3) linear moveout correction (velocity reduction) with different reduction velocities, (4) offset binning and stacking of all traces in one bin in order to reduce the number of traces and enhance signal-to-noise ratio (bin length 450 m, on average 5 traces), and (5) plotting of the sections for correlation and travel time picking.

[80] Where possible, correlations of travel time branches were checked with the reversed travel times. The layout of the profiles and the sparseness of deeper phases did not enable us to correlate reversed travel time branches directly except for the direct *Pg* phase.

[81] The velocity and structural model described in this paper is based on the following three sources:

[82] 1. The velocity distribution of the very first 3 to 5 km was determined using the ray-tracing inversion scheme by *Zelt and Smith* [1992]. The first break travel times of the reflection data were used for this inversion scheme assuming a diving wave ray path. The result is a laterally varying velocity distribution correlating with the near-surface geology. The lower velocities in the sedimentary basins of the Longitudinal Valley and the salt lakes of the Altiplano are imaged.

[83] 2. The velocity distribution of the next roughly 20 km below is well resolved by diving waves constrained by the first arrivals of the wide-angle registrations. The first arrivals were used to interactively build a velocity distribution that best fits the observed data. Forward modeling involved the ray-tracing code by *Zelt and Smith* [1992].

[84] 3. The velocities in the deeper layers below those covered by direct diving waves from the wide-angle shots cannot be resolved by the phases of the ANCORP data. Here, results from earlier investigations with longer refraction profiles were used [*Wigger et al.*, 1994; *Patzwahl et al.*, 1999; *Schmitz et al.*, 1999].

[85] **Acknowledgments.** The project ANCORP'96 was funded by the Bundesministerium für Bildung, Wissenschaft, Forschung und Technologie (BMBF, Bonn) within the German reflection seismic program DEKORP (Deutsches Kontinentales Reflexionsseismisches Programm) and by the Deutsche Forschungsgemeinschaft (DFG, Bonn) within the Collaborative Research Center 267 (SFB 267-Deformation Processes in the Andes). The support of the Chilean Navy by providing a vessel for firing the marine shots, as well as logistical support by the mining companies Compañia Minera Punta de Lobos S.A., Compañia Minera Doña Inés de Collahuasi, Compañia Quebrada Blanca, and by the local authorities Carabineros de Chile, Zona de Tarapacá y Antofagasta (Retenes de Ollagüe, Ujina), Instituto Geográfico Militar La Paz and Ministerio de Hacienda y Desarrollo Económico, Secretaria Nacional de Minera, Bolivia, is gratefully acknowledged. Seismic equipment was provided by the Geophysical Instruments Pool Potsdam and by the FU Berlin. A great deal of success is due to the more than hundred helpers and field operators from all three countries. We wish to thank David Hindle for his comments, which helped to improve an earlier version of the manuscript. Last not least, the manuscript has benefited substantially from thoughtful and constructive reviews by Ron Hyndman and two anonymous reviewers, which is gratefully acknowledged.

References

Allmendinger, R. W., and T. Gubbels, Pure and simple shear plateau uplift, Altiplano-Puna, Argentina and Bolivia, in *Geodynamics of the Andes*, edited by J. F. Dewey and S. H. Lamb, *Tectonophysics*, *259*, 1–13, 1996.

Allmendinger, R. W., and T. R. Zapata, The footwall ramp of the Subandean decollement, northernmost Argentina, from extended correlation of seismic reflection data, *Tectonophysics*, *321*, 37–55, 2000.

Allmendinger, R. W., T. E. Jordan, S. Kay, and B. L. Isacks, The evolution of the Altiplano-Puna Plateau of the central Andes, *Annu. Rev. Earth Planet. Sci.*, *25*, 139–174, 1997.

ANCORP Working Group, Seismic reflection image revealing offset of Andean subduction-zone earthquake locations into oceanic mantle, *Nature*, *397*, 341–344, 1999.

Angermann, D., J. Klotz, and C. Reigber, Space-geodetic estimation of the Nazca-South America Euler vector, *Earth Planet. Sci. Lett.*, *171*, 329–334, 1999.

Babeyko, A. Y., S. V. Sobolev, R. B. Trumbull, O. Oncken, and L. L. Lavier, Numerical models of crustal scale convection and partial melting beneath the Altiplano-Puna plateau, *Earth Planet. Sci. Lett.*, *199*, 373–388, 2002.

Baby, P., P. Rochat, G. Mascle, and G. Herail, Neogene shortening contribution to crustal thickening in the back arc of the central Andes, *Geology*, *25*, 883–886, 1997.

Baker, M. C. W., and P. W. Francis, Upper Cenozoic volcanism in the central Andes: Ages and volumes, *Earth Planet. Sci. Lett.*, *41*, 175–187, 1978.

Beck, S. L., G. Zandt, S. C. Myers, T. C. Wallace, P. G. Silver, and L. Drake, Crustal-thickness variation in the central Andes, *Geology*, *24*, 407–410, 1996.

Bock, G., B. Schurr, and G. Asch, High-resolution image of the oceanic Moho in the subducting Nazca plate from P-S converted waves, *Geophys. Res. Lett.*, *27*, 3929–3932, 2002.

Brasse, H., P. Lezaeta, V. Rath, K. Schwalenberg, W. Soyer, and V. Haak, The Bolivian Altiplano conductivity anomaly, *J. Geophys. Res.*, *107*(B5), 2096, doi:10.1029/2001JB000391, 2002.

Brown, L. D., W. Zhao, K. D. Nelson, M. Hauck, D. Alsdorf, A. Ross, M. Logan, M. Clark, X. Liu, and J. Che, Bright spots, structure, and magmatism in southern Tibet from INDEPTH seismic reflection profiling, *Science*, *274*, 1688–1690, 1996.

Buske, S., S. Lüth, H. Meyer, R. Patzig, C. Reichert, S. Shapiro, P. Wigger, and M. Yoon, Broad depth range seismic imaging of the subducted Nazca Slab, north Chile, *Tectonophysics*, *350*, 273–282, 2002.

Cahill, T., and B. L. Isacks, Seismicity and shape of the subducted Nazca plate, *J. Geophys. Res.*, *97*, 17,503–17,529, 1992.

Chmielowski, J., G. Zandt, and C. Haberland, The central Andean Altiplano-Puna magma body, *Geophys. Res. Lett.*, *26*, 783–786, 1999.

CINCA Working Group, Results of the marine geo-science survey SO-104/CINCA, paper presented at VIII Congreso Geologico Chileno, Univ. Católica del Norte, Antofagasta, Chile, 4–8 Aug. 1997.

Clowes, R. M., C. J. Yorath, and R. D. Hyndman, Reflection mapping across the convergent margin of western Canada, *Geophys. J. R. Astron. Soc.*, *89*, 79–84, 1987.

Comte, D., and G. Suárez, Stress distribution and geometry of the subducting Nazca plate in northern Chile using teleseismically recorded earthquakes, *Geophys. J. Int.*, *122*, 419–440, 1995.

Comte, D., S. W. Roecker, and G. Suárez, Velocity structure in northern Chile: Evidence of subducted oceanic crust in the Nazca Plate, *Geophys. J. Int.*, *117*, 625–639, 1994.

Comte, D., L. Dorbath, M. Pardo, T. Monfret, H. Haessler, L. Rivera, M. Frogneux, B. Glass, and C. Meneses, A double-layered seismic zone in Arica, northern Chile, *Geophys. Res. Lett.*, *26*, 1965–1968, 1999.

Delouis, B., H. Philip, L. Dorbath, and A. Cisternas, Recent crustal deformation in the Antofagasta region (northern Chile) and the subduction process, *Geophys. J. Int.*, *132*, 302–338, 1998.

DeMets, C., R. G. Gordon, D. F. Argus, and S. Stein, Current plate motions, *Geophys. J. Int.*, *101*, 425–478, 1990.

Dewey, J. F., and J. M. Bird, Mountain belts and the new global tectonics, *J. Geophys. Res.*, *75*, 2625–2627, 1970.

Gelchinsky, B., The formulae for the calculation of the Fresnel zones or volumes, *Z. Geophys.*, *57*, 33–41, 1985.

Giese, P., E. Scheuber, F. Schilling, M. Schmitz, and P. Wigger, Crustal thickening processes in the central Andes and the different nature of the Moho discontinuity, *J. S. Am. Earth Sci.*, *12*, 201–210, 1999.

Goetze, H.-J., and A. Kirchner, Interpretation of gravity and geoid in the central Andes between 20° and 29°S, *J. S. Am. Earth Sci.*, *10*, 179–188, 1997.

Graeber, F. M., and G. Asch, Three-dimensional models of *P* wave velocity and *P*-to-*S* velocity ratio in the southern central Andes by simultaneous inversion of local earthquake data, *J. Geophys. Res.*, *104*, 20,237–20,256, 1999.

Green, A. G., R. M. Clowes, C. J. Yorath, C. Spencer, E. R. Kanasewich, M. T. Brandon, and A. SoutherlandBrown, Seismic reflection imaging of the subducting Juan de Fuca plate, *Nature*, *319*, 210–213, 1986.

Griffiths, L.-J., F.-R. Smolka, and L.-D. Trembly, Adaptive deconvolution: A new technique for processing time-varying seismic data, *Geophysics*, *42*, 742–759, 1977.

Gulunay, N., FXDECON and complex Wiener prediction filter, in *Deconvolution*, *Geophys. Reprint Ser.*, vol. 17, edited by A. Robinson-Enders and O.-M. Osman, pp. 552–554, Soc. of Explor. Geophys., Tulsa, Okla., 1996.

Haberland, C., and A. Rietbrock, Attenuation tomography in the western central Andes: A detailed insight into the structure of a magmatic arc, *J. Geophys. Res.*, *106*, 11,151–11,167, 2001.

Haschke, M., W. Siebel, A. Günther, and E. Scheuber, Repeated crustal thickening and recycling during the Andean orogeny in north Chile (21–26°S), *J. Geophys. Res.*, *107*(B1), 2019, doi:10.1029/2001JB000328, 2002.

Hindle, D., J. Kley, E. Klosko, S. Stein, T. Dixon, and E. Norabuena, Consistency of geologic and geodetic displacements during Andean orogenesis, *Geophys. Res. Lett.*, *29*(8), 1188, doi:10.1029/2001GL013757, 2002.

Isacks, B., J. Oliver, and L. R. Sykes, Seismology and the new global tectonics, *J. Geophys. Res.*, *73*, 5855–5899, 1968.

Isacks, B.-L., Uplift of the central Andean Plateau and bending of the Bolivian Orocline, *J. Geophys. Res.*, *93*, 3211–3231, 1988.

James, D. E., Plate tectonic model for the evolution of the central Andes, *Geol. Soc. Am. Bull.*, *82*, 3325–3346, 1971.

Kay, R. W., and S. M. Kay, Delamination and delamination magmatism, *Tectonophysics*, *219*, 177–189, 1993.

Kirby, S. H., E. R. Engdahl, and R. P. Denlinger, Intermediate-depth intraslab earthquakes and arc volcanism as physical expressions of crustal and uppermost mantle metamorphism in subducting slabs, in *Subduction Top to Bottom*, *Geophys. Monogr. Ser.*, vol. 96, edited by G. E. Bebout et al., pp. 195–214, AGU, Washington, D. C., 1996.

Kley, J., and C. R. Monaldi, Tectonic shortening and crustal thickness in the central Andes: How good is the correlation?, *Geology*, *26*, 723–726, 1998.

Kley, J., C. R. Monaldi, and J. A. Salfity, Along-strike segmentation of the Andean foreland: Causes and consequences, *Tectonophysics*, *301*, 75–94, 1999.

Klotz, J., et al., GPS-derived deformation of the central Antofagasta M_w = 8.0 earthquake, *Pure Appl. Geophys.*, *154*, 709–730, 1999.

Kong, S. M., R. A. Phinney, and K. Roy-Chowdhury, A nonlinear signal detector for enhancement of noisy seismic record sections, *Geophysics*, *50*, 539–550, 1985.

Lamb, S., Active deformation in the Bolivian Andes, South America, *J. Geophys. Res.*, *105*, 25,627–25,653, 2000.

Lamb, S., and L. Hoke, Origin of the high plateau in the central Andes, Bolivia, South America, *Tectonics*, *16*, 623–649, 1997.

Lamb, S., L. Hoke, L. Kennan, and J. Dewey, Cenozoic evolution of the central Andes in Bolivia and northern Chile, in *Orogeny Through Time*, edited by J. P. Burg and M. Ford, *Geol. Soc. Spec. Publ.*, *121*, 237–264, 1997.

Lezaeta, P., Distortion analysis and 3-D modeling of magnetotelluric data in the Southern central Andes, Ph.D. thesis, Fac. of Geosci., Free Univ., Berlin, 2001.

Lucassen, F., S. Lewerenz, G. Franz, J. Viramonte, and K. Mezger, Metamorphism, isotopic ages and composition of lower crustal granulite xenoliths from the Cretaceous Salta Rift, Argentina, *Contrib. Mineral. Petrol.*, *134*, 325–341, 1999.

Makovsky, Y., and S. L. Klemperer, Measuring the seismic properties of Tibetan bright spots: Evidence for free aqueous fluids in the Tibetan middle crust, *J. Geophys. Res.*, *104*, 10,795–10,825, 1999.

Myers, S. C., S. Beck, G. Zandt, and T. Wallace, Lithospheric-scale structure across the Bolivian Andes from tomographic images of velocity and attenuation for P and S waves, *J. Geophys. Res.*, *103*, 21,233–21,252, 1998.

Nelson, K. D., et al., Partially molten middle crust beneath southern Tibet: Synthesis of Project INDEPTH results, *Science*, *274*, 1684–1688, 1996.

Patzwahl, R., J. Mechie, A. Schulze, and P. Giese, Two-dimensional velocity models of the Nazca plate subduction zone between 19.5°S and 25°S from wide angle seismic measurements during the CINCA95 project, *J. Geophys. Res.*, *104*, 7293–7317, 1999.

Pawley, A. R., and J. R. Holloway, Water sources for subduction zone volcanism: New experimental constraints, *Science*, *260*, 664–667, 1993.

Peacock, S. M., Thermal effect of metamorphic fluids in subduction zones, *Geology*, *15*, 1057–1060, 1997.

Peacock, S. M., and R. D. Hyndman, Hydrous minerals in the mantle wedge and the maximum depth of subduction thrust earthquakes, *Geophys. Res. Lett.*, *26*, 2517–2520, 1999.

Reutter, K.-J., E. Scheuber, and P.-J. Wigger (Eds.), *Tectonics of the Southern Central Andes: Structure and Evolution of an Active Continental Margin*, 333 pp, Springer-Verlag, New York, 1994.

Reutter, K. J., E. Scheuber, and G. Chong, The Precordilleran fault system of Chuquicamata, northern Chile: Evidence for reversals along arc-parallel strike-slip faults, *Tectonophysics*, *259*, 213–228, 1996.

Rietbrock, A., and C. Haberland, A tear in the subducting Nazca slab: Evidence from local earthquake tomography and high precision hypocenters, *Eos Trans. AGU*, *82*(47), Fall Meet. Suppl., Abstract T31A-0822, 2001.

Romanyuk, T., H.-J. Götze, and P. F. Halvorson, A density model of the Andean subduction zone, *Leading Edge*, *18*, 264–268, 1999.

Rutland, R. W. R., Andean orogeny and ocean floor spreading, *Nature*, *233*, 252–255, 1971.

Scheuber, E., and P. Giese, Architecture of the central Andes-A compilation of geoscientific data along a transect at 21°S, *J. S. Am. Earth Sci.*, *12*, 103–107, 1999.

Scheuber, E., C. T. Bogdanic, A. I. Jensen, and K. J. Reutter, Tectonic development of the North Chilean Andes in relation to plate convergence and magmatism since the Jurassic, in *Tectonics of the Southern Central Andes: Structure and Evolution of an Active Continental Margin*, edited by K. J. Reutter, E. Scheuber, and P. J. Wigger, pp. 121–139, Springer-Verlag, New York, 1994.

Schilling, F. R., and G. M. Partzsch, Quantifying partial melt fraction in the crust beneath the central Andes and the Tibetan Plateau, *Phys. Chem. Earth*, *26*, 239–246, 2001.

Schmitz, M., and J. Kley, The geometry of the central Andean backarc crust. Joint interpretation of cross-section balancing and seismic refraction data, *J. S. Am. Earth Sci.*, *10*, 99–110, 1997.

Schmitz, M., et al., crustal structure of the central Andean forearc and magmatic arc as derived from seismic studies—The PISCO 94 experiment in northern Chile (21–23°S), *J. S. Am. Earth Sci.*, *12*, 237–260, 1999.

Schurr, B., Seismic structure of the central Andean subduction zone from local earthquake data, Ph.D. thesis, Free Univ., Berlin, 2000.

Schurr, B., G. Asch, A. Rietbrock, R. Kind, M. Pardo, B. Heit, and T. Monfret, Seismicity and average velocity beneath the Argentine Puna Plateau, *Geophys. Res. Lett.*, *26*, 3025–3028, 1999.

Schwalenberg, K., V. Rath, and V. Haak, Sensitivity studies applied to a 2–D resistivity model from the central Andes, *Geophys. J. Int.*, *150*, 673–686, 2002.

Sobolev, S. V., and A. Y. Babeyko, Modelling of mineralogical composition, density and elastic wave velocities in anhydrous magmatic rocks, *Surv. Geophys.*, *15*, 515–544, 1994.

Somoza, R., Updated Nazca (Farallon)-South America relative motions during the last 40 My: Implications for mountain building in the central Andean region, *J. S. Am. Earth Sci.*, *11*, 211–215, 1998.

Soubaras, R., Explicit 3-D migration using equiripple polynomial expansion and Laplacian synthesis, *Geophysics*, *61*, 1386–1393, 1996.

Springer, M., Interpretation of heat-flow density in the central Andes, *Tectonophysics*, *306*, 377–395, 1999.

Swenson, J. L., S. L. Beck, and G. Zandt, Crustal structure of the Altiplano from broadband regional waveform modeling: Implications for the composition of thick continental crust, *J. Geophys. Res.*, *105*, 607–621, 2000.

Taner, M. T., F. Koehler, and R. E. Sheriff, Complex seismic trace analysis, *Geophysics*, *44*, 1041–1063, 1979.

Trumbull, R. B., R. Wittenbrink, K. Hahne, R. Emmermann, W. Büsch, H. Gerstenberger, and W. Siebel, Evidence for Late Miocene to Recent contamination of arc andesites by crustal melts in the Chilean Andes (25–26°S) and its geodynamic implications, *J. S. Am. Earth Sci.*, *12*, 135–155, 1999.

van der Lee, S., D. James, and P. Silver, Upper mantle S velocity structure of central and western South America, *J. Geophys. Res.*, *106*, 30,821–30,835, 2001.

Vdovin, O., J. A. Rial, A. Levshin, and M. Ritzwoller, Group-velocity tomography of South America and the surrounding oceans, *Geophys. J. Int.*, *136*, 324–340, 1999.

Von Huene, R., and D. W. Scholl, Observations at convergent margins concerning sediment subduction, subduction erosion, and the growth of continental crust, *Rev. Geophys.*, *29*, 279–316, 1991.

Von Huene, R., W. Weinrebe, and F. Heeren, Subduction erosion along the north Chile margin, *J. Geodyn.*, *27*, 345–358, 1999.

Wigger, P., et al., Variation of the crustal structure of the southern central Andes deduced from seismic refraction investigations, in *Tectonics of the Southern Central Andes*, edited by K.-J. Reutter, E. Scheuber, and P. Wigger, pp. 23–48, Springer-Verlag, New York, 1994.

Yuan, X., S. V. Sobolev, R. Kind, O. Oncken, and Andes Seismology Group, New constraints on subduction and collision processes in the central Andes from comprehensive observations of P to S converted seismic phases, *Nature*, *408*, 958–961, 2000.

Yuan, X., S. V. Sobolev, and R. Kind, Moho topography in the central Andes and its geodynamic implications, *Earth Planet. Sci. Lett.*, *199*, 389–402, 2002.

Zelt, C. A., and R. B. Smith, Seismic traveltime inversion for 2-D crustal velocity structure, *Geophys. J. Int.*, *108*, 16–34, 1992.

Ziegler, A. M., S. F. Barrett, and C. R. Scotese, Palaeoclimate, sedimentation and continental accretion, *Philos. Trans.R. Soc. London, Ser. A*, *301*, 253–264, 1981.

G. Asch, C. Haberland, J. Mechie, O. Oncken, S. Sobolev, M. Stiller, and X. Yuan, GeoForschungsZentrum Potsdam, Telegrafenberg, D-14473, Potsdam, Germany. (oncken@gfz-potsdam.de)

H. Brasse, S. Buske, P. Giese, H.-J. Götze, S. Lueth, E. Scheuber, S. Shapiro, P. Wigger, and M.-K. Yoon, Freie Universität Berlin, Malteserstr. 74-100, D-12249, Berlin, Germany.

P. Bravo and H. Vieytes, ENAP-Empresa Nacional Del Petróleo, Casilla 247, Punta Arenas, Chile.

G. Chong, G. Gonzales, and H.-G. Wilke, Universidad Católica del Norte, Avenida Angamos 0610, Antofagasta, Chile.

E. Lüschen, Universitaet München (LMU), Theresienstr. 41, D-80333, München, Germany.

E. Martinez, Chaco-SA, Km 2 1/2 Carretera Antigua a Cbba., Santa Cruz, Bolivia.

R. Rössling, SERGEOMIN, Casilla 2729, La Paz, Bolivia.

E. Ricaldi, Universidad Mayor de San Andres, Casilla 4836, La Paz, Bolivia.

A. Rietbrock, Institute of Geosciences, University of Potsdam, D-14415 Potsdam, Germany.